

## **Supporting Information (SI Appendix)**

### **Warm spring reduced carbon cycle impact of the 2012 US summer drought**

(Sebastian Wolf *et al.*, ETH Zurich, [sewolf@ethz.ch](mailto:sewolf@ethz.ch))

#### **This file includes:**

**Supporting Text**

**Supporting Tables S1–S10**

**Supporting Figures S1–S16**

**Supporting References**

## Supporting Text

### SI Methods

**Representativeness of flux tower measurements.** Large-scale measurement networks of biosphere-atmosphere exchange provide direct evidence of the carbon and water cycle response to climate anomalies at ecosystem scale (1). We used 22 flux tower sites that represent the major ecoregions and climates across the CONUS (**Fig. S2 and Table S1**). Eddy-covariance (EC) flux tower measurements are direct integrations of whole ecosystems and fluxes are measured continuously compared to regular sampling (time for space substitution). Thus, flux tower measurements are representative for ecosystems in much larger areas with similar biotic and abiotic conditions (2), such as defined by the ecoregion concept that distinguishes ecological regions at various scales (3). Flux tower measurements are the only direct measurements of biosphere-atmosphere exchange in carbon, water and energy fluxes. Regional, continental and global networks (such as AmeriFlux or FLUXNET) of these measurements are a powerful tool and the currently best available method to study ecosystem fluxes and, when combined with observations from satellite remote sensing, can be used to upscale the ecosystem response to changes in climate or disturbances at larger scales (1). The flux towers used in our synthesis sampled seven out of the ten Level I ecoregions or 97% of the ecoregion type area across CONUS (**Table S1**). Among these, the largest (**Table S6**) and most drought-affected (**Table S5B**) ecoregions were well-represented with several flux tower sites, except the North American Deserts ecoregion (one site only).

**Drought indices data.** Besides precipitation measured at the tower sites, we also evaluated Standardized Precipitation Index (SPI) data that were provided at the site-scale by the High Plains Regional Climate Center (HPRCC) based on long-term precipitation records from nearby meteorological stations. However, these SPI data could not consistently detect drought at the individual site level across all sites due to the high spatial variability of precipitation resulting in inconsistencies with measured precipitation at some sites, particularly in the Southwest but also in the Northeast. SPI data also had limited and non-significant predictive power for observed anomalies in carbon fluxes, largely related to differences in reference period between site data for fluxes (2008–2010) and precipitation data from nearby stations (at least 30 years). Consequently, we only used SPI data to quantify drought at regional and continental scales and, across ensembles of multiple sites (see **Fig. S4**). To avoid location based biases and differences in baseline at the site level (see SPI) we used the Evaporative Stress Index (ESI) as drought indicator, directly derived from site data. Despite general limitations of energy balance closure with EC measurements (4), we reduced the potential influence on Evaporative Fraction (EF) by calculating available energy as the sum of LE and H.

**Choice of atmospheric inverse model (CTE2014 vs. CT2013B).** We also evaluated inverse modeling estimates from NOAA's CarbonTracker (CT2013B) (5, 6). However, the prior biosphere model used in CT2013B (CASA-GFED2/GFED3) uses a monthly, prognostic phenology, which resolves sub-monthly changes in phenology only to a limited extent and thus cannot accurately detect anomalies during spring. In contrast, CTE2014 (7) is based on the prior biosphere model SiBCASA-GFED4, which uses a daily, diagnostic phenology based on growing degree days to better resolve phenological changes. This difference played a role for the warm

year 2012, when higher temperatures during winter and spring caused early leaf-out and carbon uptake. SiBCASA-GFED4 partially predicted these shifts in phenology with an earlier start of carbon uptake, and this signal was subsequently strongly increased through the assimilation of CO<sub>2</sub> observations with CTE2014. CT2013B with its CASA-GFED2 prior and close-to-neutral monthly mean carbon uptake in spring did not show this same anomaly. Using CTE2014 was thus better suited for analyzing the continental-scale net carbon cycle impact of concurrently warm spring and summer drought in 2012. Unlike during spring (due to differences in model phenology), net carbon uptake reductions estimated by CT2013B across CONUS during summer 2012 ( $-0.25 \text{ Pg C season}^{-1}$ ,  $-30\%$ ) were similar to those estimated by CTE2014 ( $-0.23 \text{ Pg C season}^{-1}$ ,  $-37\%$ ).

To provide an uncertainty estimate for the 2012 NEP fluxes from CTE2014, we used the independent CarbonTracker model run CTE2015, which is different from CTE2014 in minor aspects such as fossil fuel emissions, observation density over North America, and the source of three-hourly prior biosphere fluxes. Baseline estimates from the CTE2015 run were very similar to CTE2014 across CONUS and the differences for 2012 are shown in **Fig. 3H**.

### **Economic impact of the 2012 drought**

The 2012 drought caused substantial economic damage, in particular for agricultural production. Large areas of crops failed across the Great Plains and the Midwest: corn yields were the lowest since 1995 and 26% below early seasonal projections, and soybean yields were the lowest since 2003 and 10% below projections (8, 9). The extensive drought also slowed commercial shipping, with low water levels along the Mississippi River and the western Great Lakes (10). The total costs of the 2012 drought were estimated at \$30 billion, and 123 fatalities were directly associated with the summer heat wave (11).

### **Covariance and multiple regression analyses of climatic controls**

During spring, the correlation between temperature (T) and ESI was  $r^2=0.05$  (Kendall's tau coefficient), with an  $R^2=0.20$  ( $p<0.05$ , linear regression analysis). The correlation between spring NEP and T was  $r^2=0.38$ , and  $r^2=-0.15$  between spring NEP and ESI (note: like precipitation, NEP and ESI were negatively correlated during spring – see **Fig. S3**). Adding the climatic control of ESI to T in a multiple linear regression analysis (MLR, considering interactions) increased  $R^2$  from 0.29 to 0.54, although NEP~ESI itself were not significantly correlated.

During summer, the correlation between T and ESI was  $r^2=0.15$ , with an  $R^2=0.02$  (n.s.). The correlation between summer NEP and ESI was  $r^2=0.44$ , and  $r^2=0.03$  between summer NEP and T. Adding the climatic control of T to ESI in a MLR (considering interactions) increased  $R^2$  from 0.64 to 0.77, although NEP~T itself were not significantly correlated. In summary, the covariance between the dominating climatic controls T and ESI only played a minor role during both spring and summer. Including the respective other control in a MLR analyses increased the predictive power of the model, suggesting confounding effects with different seasonal strength, particularly during spring.

## Biosphere-atmosphere feedbacks in the Midwest

Increased ET during spring ( $34 \pm 7$  mm season<sup>-1</sup> or  $84 \pm 16$  MJ m<sup>-2</sup> season<sup>-1</sup> or 25%, mean  $\pm$  uncertainty, **Fig. S12A**) resulted in a relative ecosystem cooling effect as shown by an increased evaporative fraction (EF, **Fig. 4B**). This effect was relatively small compared to the  $272$  MJ m<sup>-2</sup> season<sup>-1</sup> additional incoming energy ( $R_{inc}$ ), both from elevated shortwave ( $+160$  MJ m<sup>-2</sup> season<sup>-1</sup> or +10%) and longwave ( $+112$  MJ m<sup>-2</sup> season<sup>-1</sup> or +4%) incoming radiation in spring 2012. In contrast to spring, the summer ecosystem heating feedback from increased H exceeded more than four times the climatic forcing from additional  $R_{inc}$  ( $42$  MJ m<sup>-2</sup> season<sup>-1</sup> or 0.8%), which was dominated by increased shortwave incoming radiation ( $32$  MJ m<sup>-2</sup> season<sup>-1</sup> or 2%). This effect is without considering reductions in available energy (AE,  $-24$  MJ m<sup>-2</sup> season<sup>-1</sup> or -2%) or biophysical feedbacks, such as changes in albedo from senescent vegetation (-19% in EVI, **Fig. S11**). Consequently, our results suggest that 81% of the potential excess in summer heating ( $\Delta R_{inc} + \Delta H$ ) in the Midwest was contributed by the ecosystem feedback of increased  $\Delta H$  alone.

The warmer temperatures during summer 2012 in the Midwest were associated with an ecosystem feedback from reduced evaporative cooling (and thus increased H) and the climatic forcing from increased incoming energy ( $R_{inc}$ ). While increases in  $R_{inc}$  directly enhance surface temperature, increases in H have an indirect heating effect by warming the air above the surface. This air warming does not necessarily lead to a net effect on surface temperatures, as heat can also be dissipated through increases in the height of the planetary boundary layer (PBL) (12, 13). Quantifying the actual heating contribution from the ecosystem feedback during the 2012 summer drought would require the application of a PBL model (including various assumptions about changes in synoptic transport) and is beyond the scope of our analyses.

## Impact on plant physiology and species composition

For instance, the site Kansas Field Station (KFS) had among the largest annual precipitation anomaly in 2012 ( $-639$  mm, see **Table S4**) but relatively normal annual carbon uptake (see **Table S10**). The species composition at KFS is a mixture of C<sub>3</sub>- and C<sub>4</sub>-grasses and our results suggest that during 2012, the C<sub>4</sub>-grasses outcompeted the C<sub>3</sub>-grasses based on the climatic conditions. C<sub>4</sub>-plants perform better at warmer temperatures, have a higher photosynthetic capacity and higher water-use efficiency than C<sub>3</sub>-plants, which do less well during such conditions (14). During spring 2012, water-use efficiency and peak rates of photosynthetic activity at KFS were higher than all year during the baseline, which indicates a shift in species composition towards C<sub>4</sub>-grasses. Due to their higher and earlier productivity in 2012, the C<sub>4</sub>-grasses achieved the amount of typical annual carbon uptake at KFS during spring and early summer already, before the summer drought reached its peak. Consequently, the warm spring at this site more than compensated for the summer related drought reductions. Besides such direct, intermittent effects on plant ecophysiology, drought can also have longer-term carry-over effects that lead to mortality and shifts in species composition (15, 16). There are indications among the included sites that multi-year drought has a more severe impact than single year drought because of such effects on carbohydrate reserves in plant tissue (17). Further research is needed to assess the longer-term impacts of the 2012 drought such as a lagged carbon cycle response and potentially increased tree mortality.

## Impact of spring temperature and summer drought during 2001–2012

Since 2001, the years 2002, 2006 and 2011 also had below average summer precipitation across CONUS, with  $-6.9\%$ ,  $-7.0\%$  and  $-12.5\%$ , respectively (vs. 1971–2000 mean, source: NOAA-NCEI). For comparison, the year 2012 had a summer precipitation deficit of  $14.1\%$  and a  $2.6^\circ\text{C}$  warmer spring. While spring 2006 was also warmer than “normal” ( $+1.1^\circ\text{C}$ ), spring 2002 was slightly colder ( $-0.4^\circ\text{C}$ ) and spring 2011 was close to normal ( $-0.02^\circ\text{C}$ ). The carbon cycle effects during these years with summer drought across CONUS were as follows:

In 2002 (colder spring and summer drought), NEP (CTE2014) was lower during spring ( $0.44 \text{ Pg C season}^{-1}$ ,  $-18\%$ ) and summer ( $0.41 \text{ Pg C season}^{-1}$ ,  $-22\%$ ), and consequently annually ( $0.13 \text{ Pg C yr}^{-1}$ ,  $-43\%$ ). The effects on GPP (MODIS) were less pronounced, with lower GPP during spring ( $1.58 \text{ Pg C season}^{-1}$ ,  $-8\%$ ), summer ( $3.08 \text{ Pg C season}^{-1}$ ,  $0\%$ ) and annually ( $6.46 \text{ Pg C yr}^{-1}$ ,  $-2\%$ ).

In 2006 (warm spring and summer drought), NEP was normal during spring ( $0.55 \text{ Pg C season}^{-1}$ ,  $-1\%$ ), lower in summer ( $0.40 \text{ Pg C season}^{-1}$ ,  $-24\%$ ), and lower annually ( $0.06 \text{ Pg C yr}^{-1}$ ,  $-74\%$ ). The effects on GPP were less pronounced, with lower GPP during spring ( $1.69 \text{ Pg C season}^{-1}$ ,  $-2\%$ ), summer ( $2.80 \text{ Pg C season}^{-1}$ ,  $-9\%$ ) and annually ( $6.32 \text{ Pg C yr}^{-1}$ ,  $-5\%$ ).

In 2011 (normal spring and strong summer drought), NEP was normal during spring ( $0.55 \text{ Pg C season}^{-1}$ ,  $2\%$ ), lower in summer ( $0.44 \text{ Pg C season}^{-1}$ ,  $-15\%$ ), and lower annually ( $0.22 \text{ Pg C yr}^{-1}$ ,  $-6\%$ ). The effects on GPP were less pronounced, with lower GPP during spring ( $1.61 \text{ Pg C season}^{-1}$ ,  $-6\%$ ), summer ( $2.97 \text{ Pg C season}^{-1}$ ,  $-4\%$ ) and annually ( $6.32 \text{ Pg C yr}^{-1}$ ,  $-5\%$ ).

For comparison, in 2012 (very warm spring and severe summer drought), NEP was much higher during spring ( $0.76 \text{ Pg C season}^{-1}$ ,  $+41\%$ ), lower in summer ( $0.38 \text{ Pg C season}^{-1}$ ,  $-27\%$ ), and higher annually ( $0.33 \text{ Pg C yr}^{-1}$ ,  $+43\%$ ). The effects on GPP were less pronounced, with higher GPP during spring ( $1.97 \text{ Pg C season}^{-1}$ ,  $+15\%$ ), lower in summer ( $2.61 \text{ Pg C season}^{-1}$ ,  $-16\%$ ) and annually ( $6.32 \text{ Pg C yr}^{-1}$ ,  $-5\%$ ).

In summary, this comparison of years with various intensities of spring and summer climate anomalies across CONUS indicates (1) consistent reductions of carbon uptake during summer drought, (2) increased carbon uptake during very warm springs only, and (3) that the relative impacts of the seasonal climate anomalies are typically stronger for NEP than for GPP. However, the location of these climate anomalies within the US and the spatial extent of drought play a crucial role for its impact on the annual carbon balance across the country. For instance, the summer drought in 2011 was largely confined to the South/Southwest with relatively low productive ecosystems, while the more widespread 2012 drought affected the highly productive ecosystems of the Central US and Midwest, and accordingly had a much stronger impact on summer carbon uptake across CONUS. In addition, the degree of seasonal compensation largely depends on the specific climate anomalies of each year: (1) the warmth of the spring and its impact on advancing vegetation activity and thus productivity; (2) the advancement and severity of drought during summer, and the degree to which this reduces productivity.

## Supporting Tables

**Table S1. Site characteristics of the flux towers used in this synthesis.** Elevation is denoted in meter a.s.l., mean annual temperature (MAT) in °C and mean annual precipitation (MAP) in mm yr<sup>-1</sup>. Reported is the mean from the baseline period (2008–2010).

Site-Name	Site-ID	Ecoregion	IGBP	Climate	Latitude	Longitude	Elevation	MAT	MAP	Ref.
Morgan Monroe State Forest	US-MMS	ETF	DBF	Cfa	39.3232	-86.4131	275	12.2	1162	(18)
Silas Little Experimental Forest	US-Slt	ETF	DBF	Cfa	39.9137	-74.5960	30	12.3	998	(19)
Howland Forest Main	US-Ho1	ETF	ENF	Dfb	45.2041	-68.7402	60	7.0	895	(20)
Cedar Bridge	US-Ced	ETF	MF	Cfa	39.8379	-74.3791	58	12.0	1222	(19)
Bartlett Experimental Forest	US-Bar	NF	DBF	Dfb	44.0646	-71.2881	272	7.5	1356	(21)
University of Michigan Biological Station	US-UMB	NF	DBF	Dfb	45.5598	-84.7138	234	7.0	605	(22)
Park Falls	US-Pfa	NF	MF	Dfb	45.9459	-90.2723	470	5.2	577	(23)
Kansas Field Station	US-KFS	GP	GRA	Cfa	39.0561	-95.1907	333	13.4	686	(24)
Konza Prairie	US-KON	GP	GRA	Cfa	39.0824	-96.5603	443	13.9	1043	(24)
HLC Pinyon Juniper Woodland	US-Mpj	GP	OSH	BSk*	34.4384	-106.2377	2138	10.5	338	(25)
Tablelands Juniper Savanna	US-Wjs	GP	OSH	BSk*	34.4255	-105.8615	1926	12.2	283	(25)
Santa Rita Creosote	US-SRC	NAD	OSH	BSk*	31.9083	-110.8395	991	19.6	314	(26)
Santa Rita Mesquite Savanna	US-SRM	SSH	OSH	BSk*	31.8214	-110.8661	1116	18.9	345	(27)
Lucky Hills Shrubland	US-Whs	SSH	OSH	BSk*	31.7438	-110.0522	1370	17.3	272	(28)
Kendall Grassland	US-WKG	SSH	GRA	BSk*	31.7365	-109.9419	1531	17.0	298	(16)
Vaira Ranch	US-Var	MC	GRA	Csa*	38.4067	-120.9507	129	15.6	543	(29)
Tonzi Ranch	US-Ton	MC	WSA	Csa*	38.4316	-120.9660	177	16.1	552	(29)
Niwot Ridge	US-NR1	NWFM	ENF	Dfc	40.0329	-105.5464	3050	1.8	628	(30)
Valles Caldera Mixed Conifer	US-Vcm	NWFM	ENF	Cfb	35.8884	-106.5321	3003	4.5	703	(25)
Valles Caldera Ponderosa Pine	US-Vcp	NWFM	ENF	Cfb	35.8624	-106.5974	2542	6.4	538	(25)
Metolius Intermediate Pine	US-Me2	NWFM	ENF	Csb*	44.4523	-121.5574	1253	7.1	527	(31)
Metolius Young Pine	US-Me6	NWFM	ENF	Csb*	44.3232	-121.6043	996	7.8	364	(32)

\* Sites with regular, seasonal drought belong to the climates BSk, Csa and Csb

Ecoregions: ETF..Eastern Temperate Forests, NF..Northern Forests, GP..Great Plains, NAD..North American Deserts, SSH..Southern Semiarid Highlands, MC..Mediterranean California, NWFM..North-western Forested Mountains.

IGBP: DBF..Deciduous Broadleaf Forest, ENF..Evergreen Needleleaf Forest, MF..Mixed Forest, GRA..Grassland, OSH..Open Shrubland, WSA..Woody Savanna

Climate: BSk..Cold semi-arid climate, Cfa..Warm oceanic climate, Cfb..Temperate oceanic climate, Csa..Warm Mediterranean climate, Csb..Temperate Mediterranean climate, Dfa..Warm continental climate, Dfb..Temperate continental climate, Dfc..Cool continental climate

**Table S2A. Ensemble mean EC ecosystem fluxes at tower sites during baseline.**

Mean  $\pm$  standard deviation of net ecosystem production (NEP, g C m<sup>-2</sup>), gross primary production (GPP, g C m<sup>-2</sup>) and evapotranspiration (ET, mm) for all sites (n=22), for sites affected by summer drought in 2012 (n=13), and for drought sites located in the Midwest (n=3; sites US-KON, US-KFS, US-MMS) during the baseline (2008–2010).

Ensemble	Spring			Summer			Annual		
	NEP	GPP	ET	NEP	GPP	ET	NEP	GPP	ET
All (n=22)	50±87	213±117	121±44	142±130	463±334	215±97	163±139	916±475	470±161
Drought sites (n=13)	24±73	157±98	106±33	128±147	433±376	220±95	150±120	797±512	446±145
Midwest (n=3)	-30±40	235±35	137±34	273±204	896±370	348±57	154±162	1400±405	622±112

**Table S2B. Ensemble mean EC ecosystem fluxes at tower sites during 2012.**

Mean  $\pm$  standard deviation of net ecosystem production (NEP, g C m<sup>-2</sup>), gross primary production (GPP, g C m<sup>-2</sup>) and evapotranspiration (ET, mm) for all sites (n=22), for sites affected by summer drought in 2012 (n=13), and for drought sites located in the Midwest (n=3; sites US-KON, US-KFS, US-MMS) during 2012.

Ensemble	Spring			Summer			Annual		
	NEP	GPP	ET	NEP	GPP	ET	NEP	GPP	ET
All (n=22)	65±85	256±148	134±50	118±129	428±319	213±100	147±150	919±524	480±173
Drought sites (n=13)	49±66	200±141	122±45	96±148	329±283	193±80	133±148	705±423	422±119
Midwest (n=3)	72±48	377±42	171±26	119±178	460±150	266±19	85±215	1012±270	560±65

**Table S2C. Ensemble mean EC ecosystem flux anomalies at tower sites in 2012.**

Mean  $\pm$  standard deviation (SD), minimum and maximum difference (95<sup>th</sup> percentile range), mean relative anomalies (%), and uncertainties (unc)  $\pm$  SD of net ecosystem production (NEP, g C m<sup>-2</sup>), gross primary production (GPP, g C m<sup>-2</sup>) and evapotranspiration (ET, mm) for all sites (n=22), for sites affected by summer drought in 2012 (n=13), and at drought sites located in the Midwest (n=3; sites US-KON, US-KFS, US-MMS).

Ensemble	Spring			Summer			Annual			
	$\Delta$ NEP	$\Delta$ GPP	$\Delta$ ET	$\Delta$ NEP	$\Delta$ GPP	$\Delta$ ET	$\Delta$ NEP	$\Delta$ GPP	$\Delta$ ET	
All (n=22)	mean±SD	15±51	43±63	13±21	-24±87	-35±220	-1±57	-16±86	3±275	9±70
	min	-59	-41	-10	-204	-518	-104	-213	-505	-106
	max	129	168	55	94	187	104	130	408	133
	%	29%	20%	11%	-17%	-8%	-1%	-10%	0%	2%
	unc±SD	13±8	14±7	7±1	18±12	23±15	9±4	24±26	29±19	11±5
Drought sites (n=13)	mean±SD	25±57	42±66	15±20	-32±108	-104±260	-27±52	-17±106	-92±293	-25±54
	min	-44	-29	-8	-261	-683	-116	-216	-722	-108
	max	137	156	49	107	136	57	144	169	53
	%	103%	27%	14%	-25%	-24%	-12%	-11%	-12%	-6%
	unc±SD	11±7	11±7	6±2	18±14	20±16	10±5	18±11	21±12	11±6
Midwest (n=3)	mean±SD	101±50	142±22	34±25	-154±167	-436±408	-83±50	-69±133	-388±541	-63±61
	min	52	120	7	-325	-866	-129	-209	-961	-109
	max	146	158	49	-18	-160	-33	25	-34	2
	%	343%	61%	25%	-56%	-49%	-24%	-45%	-28%	-10%
	unc±SD	17±6	17±6	7±1	26±11	29±11	13±8	23±10	26±9	12±7

**Table S3. Ensemble mean anomalies in MODIS vegetation activity and ecosystem fluxes at tower sites.** Mean 2012 anomalies of enhanced vegetation index (EVI), total gross ecosystem production (GPP, g C m<sup>-2</sup>) and total evapotranspiration (ET, mm) for all sites (n=22), for sites affected by summer drought (n=13), and for drought sites located in the Midwest (n=3; sites US-KON, US-KFS, US-MMS). Anomalies are denoted absolute and relative (%) to the baseline of 2008–2010.

Region	Spring			Summer			Annual		
	ΔEVI	ΔGPP	ΔET	ΔEVI	ΔGPP	ΔET	ΔEVI	ΔGPP	ΔET
All (n=22)	0.01 (4%)	39 (18%)	7 (7%)	-0.02 (-6)	-75 (-17%)	-19 (-10%)	-0.01 (-3%)	-41 (-5%)	-21 (-5%)
Drought sites (n=13)	0.02 (11%)	41 (25%)	12 (16%)	-0.03 (-10%)	-104 (-31%)	-37 (-22%)	-0.01 (-3%)	-81 (-12%)	-41 (-11%)
Midwest (n=3)	0.06 (18%)	83 (30%)	35 (23%)	-0.11 (-19%)	-270 (-51%)	-124 (-16%)	-0.02 (-7%)	-206 (-19%)	-109 (-16%)

**Table S4. The anomalies in climate at tower sites in 2012.** Values are for 2012 relative to baseline (2008–2010) measured at flux tower sites. Reported values are anomalies for air temperature (T, °C), total precipitation (P, mm) and vapor pressure deficit (VPD, kPa) for seasons (three months) and annually (twelve months).

Ensemble	Spring			Summer			Annual		
	ΔT	ΔP	ΔVPD	ΔT	ΔP	ΔVPD	ΔT	ΔP	ΔVPD
US-MMS*	3.2	-127	0.2	1.5	-300	0.6	2	-379	0.2
US-Slt	1.7	-84	0.1	0.1	76	0.1	1.1	19	0.0
US-Ho1	0.8	28	0.0	0.2	21	0.0	0.4	47	0.0
US-Ced	1.4	-55	0.0	-0.2	69	0.0	0.9	-44	0.0
US-Bar	1.4	21	0.0	0.9	-42	0.2	1	-65	0.1
US-UMB*	2.8	1	0.0	2.3	-30	0.2	2.2	-3	0.1
US-Pfa*	3.2	102	0.0	1.4	-81	0.1	1.9	-8	0.0
US-KFS*	6.9	-119	0.4	3.9	-274	1.0	4.3	-571	0.4
US-KON*	4.4	-146	0.2	0.6	-326	0.3	1.6	-639	0.2
US-Mpj*	1.8	-39	0.2	1.1	-54	0.2	1.3	-154	0.2
US-Wjs*	1.7	2	0.2	1.6	-19	0.4	1.3	-69	0.2
US-SRC*	0.3	3	0.1	-0.1	-49	0.0	0	-94	0.1
US-SRM*	1	-11	0.2	0.1	-28	0.0	0.4	-38	0.1
US-Whs*	1.1	-4	0.2	0.6	-65	0.2	0.8	-32	0.1
US-WKG*	1.5	11	0.2	0.7	-30	0.1	1	17	0.1
US-Var	0.4	194	-0.1	0.3	3	0.1	0.6	261	0.0
US-Ton	0.2	167	0.0	0.3	1	0.1	0.5	186	0.1
US-NR1	3.4	-50	0.2	1.9	208	0.1	1.6	286	0.1
US-Vcm*	1.9	379	0.1	1.1	-39	0.1	1.3	83	0.1
US-Vcp*	2.1	-20	0.1	0	-46	0.2	1	-226	0.1
US-Me2	0.9	39	0.0	-0.3	39	0.0	0.4	191	0.0
US-Me6	0.7	61	0.0	-0.6	24	-0.1	0.1	209	0.0

\* Sites with a summer precipitation deficit of at least 10% (n=13)



**Table S5A. Large-scale variability in precipitation during 1982–2011 and baseline compared to the anomaly of 2012.** Mean  $\pm$  standard deviation of total precipitation (P, mm) during the long-term reference period 1982–2011 and the baseline of 2008–2010 compared to the mean anomalies of 2012, which are denoted absolute (mm) and relative (%) to the baseline. Data are derived from the NASA Modern-Era Retrospective Analysis for Research and Applications (MERRA).

Region	Spring			Summer			Annual		
	1982–2011	Baseline	$\Delta$ 2012	1982–2011	Baseline	$\Delta$ 2012	1982–2011	Baseline	$\Delta$ 2012
CONUS	195 $\pm$ 22	195 $\pm$ 11	–11 (–6%)	226 $\pm$ 20	233 $\pm$ 17	–42 (–18%)	742 $\pm$ 54	756 $\pm$ 30	–90 (–12%)
ETF	264 $\pm$ 42	282 $\pm$ 35	–38 (–13%)	346 $\pm$ 38	358 $\pm$ 27	–33 (–9%)	1061 $\pm$ 91	1111 $\pm$ 108	–125 (–11%)
NF	229 $\pm$ 33	202 $\pm$ 38	21 (10%)	264 $\pm$ 31	264 $\pm$ 19	–77 (–29%)	874 $\pm$ 62	854 $\pm$ 18	–92 (–11%)
GP	179 $\pm$ 24	178 $\pm$ 8	–14 (–8%)	226 $\pm$ 27	238 $\pm$ 30	–83 (–35%)	614 $\pm$ 59	631 $\pm$ 26	–148 (–23%)
NAD	86 $\pm$ 17	74 $\pm$ 17	–10 (–14%)	83 $\pm$ 20	83 $\pm$ 5	–15 (–17%)	325 $\pm$ 52	313 $\pm$ 45	–57 (–18%)
SSH	35 $\pm$ 20	17 $\pm$ 6	4 (23%)	163 $\pm$ 53	175 $\pm$ 91	–37 (–21%)	356 $\pm$ 87	332 $\pm$ 112	–79 (–45%)
MC	117 $\pm$ 70	75 $\pm$ 55	66 (87%)	13 $\pm$ 7	7 $\pm$ 7	2 (26%)	444 $\pm$ 152	456 $\pm$ 160	–25 (–6%)
NWFM	234 $\pm$ 41	226 $\pm$ 39	24 (11%)	133 $\pm$ 31	127 $\pm$ 10	–2 (–1%)	821 $\pm$ 111	791 $\pm$ 82	61 (8%)

Ecoregions: ETF..Eastern Temperate Forests, NF..Northern Forests, GP..Great Plains, NAD..North American Deserts, SSH..Southern Semiarid Highlands, MC..Mediterranean California, NWFM..North-western Forested Mountains, CONUS..Contiguous United States. Three further ecoregions of CONUS were excluded as they are not represented by site level flux tower measurements in this synthesis study, namely Marine West Coast Forests, Temperate Sierras and Tropical Wet Forests.

**Table S5B. Large-scale standardized precipitation anomalies during baseline and 2012.** Anomalies in Standardized Precipitation Index (SPI, 6 months,  $\sigma$ ) for CONUS and Ecoregions during the baseline (2008–2010) and 2012. SPI data were derived from the Global Integrated Drought Monitoring and Prediction System (GIDMaPS, <http://drought.eng.uci.edu>) and are based on MERRA precipitation data since 1980.

Region	Spring		Summer		Annual	
	Baseline	2012	Baseline	2012	Baseline	2012
CONUS	0.1	–0.2	0.2	–0.6	0.1	–0.5
ETF	0.2	–0.2	0.3	–0.7	0.1	–0.3
NF	0.1	–0.4	0.1	0.0	0.2	–0.3
GP	0.0	0.0	0.3	–0.8	0.3	–0.8
NAD	0.0	–0.7	–0.1	–0.7	–0.1	–0.6
SSH	0.2	–0.4	0.3	–0.6	0.2	–0.3
MC	0.0	–0.8	–0.4	0.0	–0.1	–0.4
NWFM	0.1	0.1	0.1	0.3	0.0	–0.1

**Table S6. Large-scale anomalies in carbon uptake and evapotranspiration.** CarbonTracker and MODIS based mean anomalies of net ecosystem production (NEP, g C m<sup>-2</sup>), gross primary production (GPP, g C m<sup>-2</sup>) and evapotranspiration (ET, mm) for CONUS and ecoregions in 2012 compared to baseline (2008–2010). NEP is estimated from atmospheric inversions of CO<sub>2</sub> mole fractions by CarbonTracker, and GPP and ET are derived from MODIS. Anomalies are denoted absolute and relative (%) to the baseline. The numbers in brackets behind region names denote the relative percentage area within CONUS.

Region	Spring			Summer			Annual		
	ΔNEP	ΔGPP	ΔET	ΔNEP	ΔGPP	ΔET	ΔNEP	ΔGPP	ΔET
CONUS (100%)	31 (46%)	35 (16%)	5 (5%)	-30 (-37%)	-76 (-19%)	-30 (-14%)	43 (52%)	-49 (-6%)	-31 (-6%)
ETF (32.2%)	69 (62%)	57 (19%)	23 (11%)	-17 (-15%)	-86 (-15%)	-35 (-10%)	77 (131%)	-18 (-2%)	-11 (-2%)
NF (4.7%)	-22 (18%)	75 (36%)	14 (12%)	-38 (-20%)	-114 (-17%)	21 (6%)	-67 (-54%)	-62 (-6%)	36 (6%)
GP (28.8%)	16 (29%)	32 (24%)	-1 (-6%)	-71 (-72%)	-123 (-36%)	-55 (-37%)	-46 (-111%)	-123 (-19%)	-69 (-18%)
NAD (18.2%)	4 (24%)	7 (17%)	-9 (-18%)	-3 (-82%)	-20 (-15%)	-11 (-17%)	5 (54%)	-16 (-6%)	-30 (-18%)
SSH (0.5%)	-19 (-86%)	-19 (-18%)	-5 (-16%)	15 (389%)	-15 (-18%)	-15 (-36%)	20 (69%)	-47 (-14%)	-35 (-25%)
MC (2.1%)	-5 (-9%)	-27 (-8%)	-5 (-5%)	-18 (-206%)	-10 (-5%)	-6 (-9%)	-84 (-878%)	-54 (-7%)	-22 (-7%)
NWFM (10.6%)	24 (58%)	32 (44%)	-7 (-7%)	0 (2%)	-29 (-8%)	-10 (-9%)	46 (91%)	2 (0%)	-17 (-5%)

**Table S7. Carbon uptake and evapotranspiration across CONUS during the last decade.** CarbonTracker (CTE2014) and MODIS based fluxes of seasonal and annual net ecosystem production (NEP, Pg C yr<sup>-1</sup>), gross primary production (GPP, Pg C yr<sup>-1</sup>) and evapotranspiration (ET, 10<sup>3</sup> km<sup>3</sup> yr<sup>-1</sup>) across the CONUS (Contiguous United States) from 2001 to 2012. NEP is estimated from atmospheric inversions of CO<sub>2</sub> concentrations by CarbonTracker, and GPP and ET are derived from MODIS. Numbers denote the mean ± interannual variability (standard deviation) during the period of 2001–2011 and during the baseline, and the fluxes during 2012. Anomalies for 2012 are shown absolute and relative (%) compared to the baseline of 2008–2010 and compared to the period of 2001–2011. The difference between the relative anomalies of both reference periods is used to estimate the potential bias for the impact of the 2012 event due to the baseline selection of this study.

CONUS	Spring			Summer			Annual		
	NEP	GPP	ET	NEP	GPP	ET	NEP	GPP	ET
<b>2001–2011</b>	0.54±0.07	1.72±0.10	0.97±0.03	0.52±0.11	3.09±0.18	1.54±0.08	0.23±0.11	6.62±0.30	3.75±0.13
<b>Baseline (2008–2010)</b>	0.52±0.10	1.69±0.12	0.97±0.05	0.61±0.09	3.20±0.14	1.61±0.09	0.22±0.05	6.70±0.25	3.80±0.13
<b>2012</b>	0.76	1.97	1.01	0.38	2.61	1.37	0.33	6.32	3.56
<b>Δ2012 (vs. Baseline)</b>	0.24 46%	0.27 16%	0.04 4%	-0.23 -37%	-0.59 -19%	-0.23 -14%	0.11 52%	-0.38 -6%	-0.24 -6%
<b>Δ2012 (vs. 2001–2011)</b>	0.22 41%	0.25 14%	0.04 4%	-0.14 -26%	-0.48 -15%	-0.17 -11%	0.10 42%	-0.31 -5%	-0.18 -5%

Estimated anomaly bias for using the baseline of 2008–2010 compared to 2001–2011: Spring: NEP +5%, GPP +2%, ET 0%; Summer: NEP +11%, GPP +4%, ET +3%; Annual: NEP +10%, GPP +1%, ET +1%.

**Table S8A. Ensemble mean climate at tower sites during baseline.** Mean  $\pm$  standard deviation of temperature (T, °C), total precipitation (P, mm) and vapor pressure deficit (VPD, kPa) for all sites (n=22), for sites affected by summer drought in 2012 (n=13), and for drought sites located in the Midwest (n=3; sites US-KON, US-KFS, US-MMS) during the baseline (2008–2010).

Ensemble	Spring			Summer			Annual		
	T	P	VPD	T	P	VPD	T	P	VPD
All (n=22)	10.2 $\pm$ 5.3	143 $\pm$ 103	0.8 $\pm$ 0.5	21.1 $\pm$ 4.5	209 $\pm$ 131	1.3 $\pm$ 0.6	11.1 $\pm$ 5.0	648 $\pm$ 329	0.8 $\pm$ 0.4
Drought sites (n=13)	11.5 $\pm$ 5.3	108 $\pm$ 102	1.0 $\pm$ 0.5	22.3 $\pm$ 4.5	240 $\pm$ 112	1.4 $\pm$ 0.6	12.1 $\pm$ 5.2	551 $\pm$ 291	0.9 $\pm$ 0.5
Midwest (n=3)	13.1 $\pm$ 0.4	247 $\pm$ 114	0.6 $\pm$ 0.1	25.3 $\pm$ 1.7	404 $\pm$ 106	1.0 $\pm$ 0.0	13.1 $\pm$ 0.9	964 $\pm$ 248	0.6 $\pm$ 0.0

**Table S8B. Ensemble mean climate at tower sites during 2012.** Mean  $\pm$  standard deviation of temperature (T, °C), total precipitation (P, mm) and vapor pressure deficit (VPD, kPa) for all sites (n=22), for sites affected by summer drought in 2012 (n=13), and for drought sites located in the Midwest (n=3; sites US-KON, US-KFS, US-MMS) during 2012.

Ensemble	Spring			Summer			Annual		
	T	P	VPD	T	P	VPD	T	P	VPD
All (n=22)	12.1 $\pm$ 5.3	159 $\pm$ 133	0.9 $\pm$ 0.5	21.9 $\pm$ 4.6	166 $\pm$ 116	1.5 $\pm$ 0.6	12.3 $\pm$ 4.9	601 $\pm$ 343	0.9 $\pm$ 0.4
Drought sites (n=13)	14.0 $\pm$ 5.2	110 $\pm$ 147	1.0 $\pm$ 0.5	23.4 $\pm$ 4.6	137 $\pm$ 56	1.7 $\pm$ 0.6	13.6 $\pm$ 4.9	389 $\pm$ 225	1.1 $\pm$ 0.5
Midwest (n=3)	18.0 $\pm$ 2.0	116 $\pm$ 108	0.6 $\pm$ 0.1	27.3 $\pm$ 2.6	104 $\pm$ 81	1.6 $\pm$ 0.3	15.7 $\pm$ 1.8	434 $\pm$ 335	0.9 $\pm$ 0.1

**Table S8C. Ensemble mean climate anomalies at tower sites in 2012.** Mean  $\pm$  standard deviation, minimum and maximum difference (95<sup>th</sup> percentile range), and mean relative anomalies (%) of temperature (T, °C), total precipitation (P, mm) and vapor pressure deficit (VPD, kPa) for all sites (n=22), for sites affected by summer drought in 2012 (n=13), and for drought sites located in the Midwest (n=3; sites US-KON, US-KFS, US-MMS) relative to the baseline of 2008–2010.

Ensemble		Spring			Summer			Annual		
		$\Delta$ T	$\Delta$ P	$\Delta$ VPD	$\Delta$ T	$\Delta$ P	$\Delta$ VPD	$\Delta$ T	$\Delta$ P	$\Delta$ VPD
All (n=22)		1.9 $\pm$ 1.6	16 $\pm$ 117	0.1 $\pm$ 0.1	0.8 $\pm$ 1.0	-43 $\pm$ 122	0.2 $\pm$ 0.2	1.2 $\pm$ 0.9	-47 $\pm$ 239	0.1 $\pm$ 0.1
	min	0.2	-135	-0.1	-0.4	-311	-0.1	0.0	-599	0.0
	max	5.7	290	0.3	3.1	145	0.8	3.3	274	0.3
	%	19%	11%	13%	4%	-20%	14%	10%	-7%	12%
Drought sites (n=13)		2.4 $\pm$ 1.7	2 $\pm$ 132	0.2 $\pm$ 0.1	1.1 $\pm$ 1.1	-103 $\pm$ 114	0.3 $\pm$ 0.3	1.5 $\pm$ 1.1	-162 $\pm$ 230	0.1 $\pm$ 0.1
	min	0.5	-140	0.0	0.0	-317	0.0	0.1	-616	0.0
	max	6.2	303	0.3	3.5	-22	0.9	3.7	65	0.3
	%	21%	2%	17%	5%	-43%	19%	12%	-29%	15%
Midwest (n=3)		4.8 $\pm$ 1.9	-131 $\pm$ 14	0.3 $\pm$ 0.1	2.0 $\pm$ 1.7	-300 $\pm$ 26	0.6 $\pm$ 0.3	2.6 $\pm$ 1.5	-530 $\pm$ 135	0.2 $\pm$ 0.1
	min	3.2	-145	0.2	0.6	-325	0.3	1.6	-635	0.2
	max	6.8	-119	0.4	3.8	-275	1.0	4.2	-388	0.4
	%	37%	-53%	41%	8%	-74%	64%	20%	-55%	41%

**Table S9. Ensemble mean MERRA precipitation at tower sites during 1982–2011 and baseline compared to the anomaly of 2012.** Mean  $\pm$  standard deviation of total precipitation (P, mm) for all sites (n=22), for sites affected by summer drought in 2012 (n=13), and for drought sites located in the Midwest (n=3; sites US-KON, US-KFS, US-MMS) during 1982–2011 and the baseline of 2008–2010 compared to the mean anomalies of 2012, which are denoted absolute (mm) and relative (%) to the baseline. Data are derived from the NASA Modern-Era Retrospective Analysis for Research and Applications (MERRA).

Ensemble	Spring			Summer			Annual		
	1982–2011	Baseline	$\Delta$ 2012	1982–2011	Baseline	$\Delta$ 2012	1982–2011	Baseline	$\Delta$ 2012
All (n=22)	188 $\pm$ 52	181 $\pm$ 30	3 (0%)	196 $\pm$ 52	205 $\pm$ 64	-53 (-13%)	746 $\pm$ 110	753 $\pm$ 100	-55 (-14%)
Drought sites (n=13)	117 $\pm$ 37	110 $\pm$ 24	-15 (-12%)	191 $\pm$ 57	205 $\pm$ 78	-76 (-36%)	513 $\pm$ 89	519 $\pm$ 82	-124 (-26%)
Midwest (n=3)	237 $\pm$ 56	253 $\pm$ 34	-44 (-11%)	266 $\pm$ 42	294 $\pm$ 46	-135 (-44%)	826 $\pm$ 107	865 $\pm$ 47	-197 (-25%)

**Table S10. EC ecosystem flux anomalies at tower sites in 2012.** Mean  $\pm$  uncertainties of 2012 anomalies in net ecosystem production (NEP, g C m<sup>-2</sup>), gross primary production (GPP, g C m<sup>-2</sup>) and evapotranspiration (ET, mm) relative to the baseline of 2008–2010.

Ensemble	Spring			Summer			Annual		
	NEP	GPP	ET	NEP	GPP	ET	NEP	GPP	ET
US-MMS*	147 $\pm$ 23	151 $\pm$ 24	49 $\pm$ 6	-110 $\pm$ 35	-248 $\pm$ 36	-31 $\pm$ 11	-13 $\pm$ 33	-123 $\pm$ 32	6 $\pm$ 8
US-Slt	-32 $\pm$ 16	26 $\pm$ 24	-1 $\pm$ 6	34 $\pm$ 28	191 $\pm$ 49	45 $\pm$ 15	-5 $\pm$ 27	275 $\pm$ 79	52 $\pm$ 14
US-Ho1	23 $\pm$ 16	41 $\pm$ 17	22 $\pm$ 6	-6 $\pm$ 26	35 $\pm$ 34	105 $\pm$ 8	10 $\pm$ 23	54 $\pm$ 31	126 $\pm$ 10
US-Ced	3 $\pm$ 17	56 $\pm$ 21	-9 $\pm$ 7	44 $\pm$ 22	183 $\pm$ 33	103 $\pm$ 11	60 $\pm$ 22	334 $\pm$ 54	112 $\pm$ 10
US-Bar	-12 $\pm$ 18	7 $\pm$ 20	14 $\pm$ 9	-43 $\pm$ 33	-7 $\pm$ 43	35 $\pm$ 9	-69 $\pm$ 43	10 $\pm$ 52	78 $\pm$ 16
US-UMB*	32 $\pm$ 17	52 $\pm$ 19	0 $\pm$ 5	125 $\pm$ 39	73 $\pm$ 43	66 $\pm$ 10	162 $\pm$ 30	98 $\pm$ 34	57 $\pm$ 8
US-Pfa*	24 $\pm$ 19	69 $\pm$ 19	16 $\pm$ 8	60 $\pm$ 45	159 $\pm$ 51	21 $\pm$ 15	68 $\pm$ 36	196 $\pm$ 45	43 $\pm$ 13
US-KFS*	49 $\pm$ 11	158 $\pm$ 11	5 $\pm$ 5	-13 $\pm$ 14	-156 $\pm$ 17	-85 $\pm$ 7	27 $\pm$ 13	-30 $\pm$ 16	-111 $\pm$ 7
US-KON*	108 $\pm$ 17	118 $\pm$ 17	49 $\pm$ 8	-338 $\pm$ 30	-903 $\pm$ 35	-131 $\pm$ 22	-220 $\pm$ 24	-1011 $\pm$ 30	-83 $\pm$ 21
US-Mpj*	28 $\pm$ 5	32 $\pm$ 5	-8 $\pm$ 5	-15 $\pm$ 5	-79 $\pm$ 6	-48 $\pm$ 5	-8 $\pm$ 6	-92 $\pm$ 6	-63 $\pm$ 5
US-Wjs*	-10 $\pm$ 4	1 $\pm$ 5	0 $\pm$ 5	10 $\pm$ 5	-17 $\pm$ 6	5 $\pm$ 6	-42 $\pm$ 6	-96 $\pm$ 7	-17 $\pm$ 6
US-SRC*	-14 $\pm$ 5	-13 $\pm$ 7	17 $\pm$ 7	-13 $\pm$ 6	-42 $\pm$ 8	-39 $\pm$ 6	-20 $\pm$ 21	-66 $\pm$ 27	-34 $\pm$ 20
US-SRM*	-10 $\pm$ 5	-10 $\pm$ 5	12 $\pm$ 5	-5 $\pm$ 7	-49 $\pm$ 8	-23 $\pm$ 7	22 $\pm$ 20	8 $\pm$ 22	-7 $\pm$ 19
US-Whs*	-17 $\pm$ 3	-26 $\pm$ 6	-9 $\pm$ 5	-28 $\pm$ 5	-35 $\pm$ 7	-15 $\pm$ 6	-43 $\pm$ 5	-48 $\pm$ 11	-29 $\pm$ 6
US-WKG*	-37 $\pm$ 3	-31 $\pm$ 4	4 $\pm$ 5	-3 $\pm$ 6	38 $\pm$ 7	35 $\pm$ 7	-40 $\pm$ 5	47 $\pm$ 8	40 $\pm$ 7
US-Var	-7 $\pm$ 15	26 $\pm$ 22	10 $\pm$ 8	-2 $\pm$ 6	-11 $\pm$ 9	3 $\pm$ 3	-32 $\pm$ 12	-8 $\pm$ 34	-14 $\pm$ 7
US-Ton	-75 $\pm$ 12	-56 $\pm$ 12	-12 $\pm$ 7	-29 $\pm$ 11	-33 $\pm$ 12	6 $\pm$ 4	-78 $\pm$ 14	-95 $\pm$ 15	-12 $\pm$ 8
US-NR1	50 $\pm$ 9	84 $\pm$ 10	-8 $\pm$ 6	-41 $\pm$ 16	27 $\pm$ 20	-3 $\pm$ 7	-2 $\pm$ 13	114 $\pm$ 16	-14 $\pm$ 8
US-Vcm*	70 $\pm$ 9	63 $\pm$ 9	43 $\pm$ 9	-3 $\pm$ 13	-15 $\pm$ 14	-46 $\pm$ 14	96 $\pm$ 12	70 $\pm$ 13	-23 $\pm$ 11
US-Vcp*	-47 $\pm$ 18	-12 $\pm$ 18	21 $\pm$ 7	-89 $\pm$ 18	-80 $\pm$ 21	-60 $\pm$ 9	-208 $\pm$ 23	-151 $\pm$ 27	-103 $\pm$ 9
US-Me2	38 $\pm$ 37	177 $\pm$ 26	61 $\pm$ 9	-91 $\pm$ 21	116 $\pm$ 37	2 $\pm$ 10	-69 $\pm$ 130	475 $\pm$ 63	140 $\pm$ 11
US-Me6	12 $\pm$ 14	33 $\pm$ 16	11 $\pm$ 6	27 $\pm$ 12	84 $\pm$ 16	28 $\pm$ 6	51 $\pm$ 20	113 $\pm$ 23	54 $\pm$ 11

\* Sites with a summer precipitation deficit of at least 10% (n=13)

## Supporting Figures

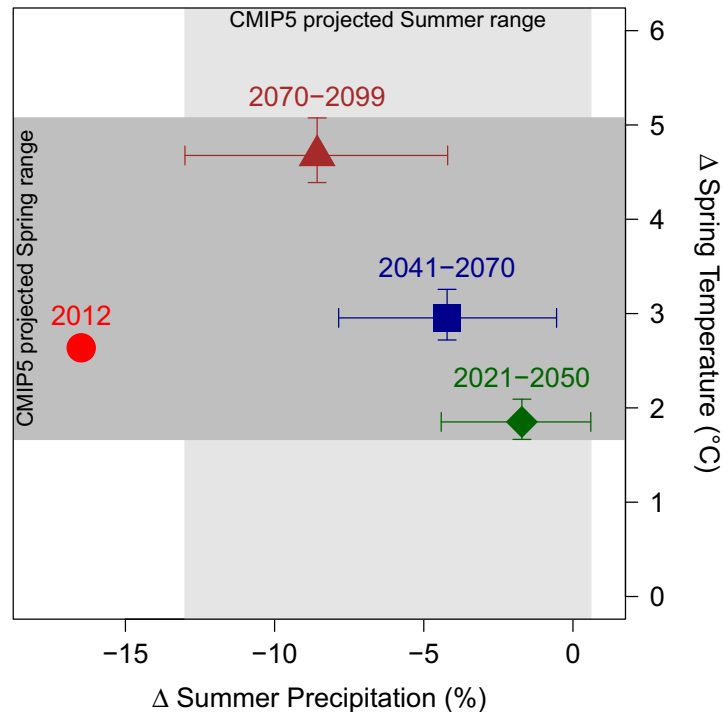


**Fig. S1. The seasonal anomalies of 2012 compared to future climate projections across the Contiguous US.** Mean seasonal anomalies of spring temperature ( $^{\circ}\text{C}$ ) and summer precipitation (%) measured across CONUS in 2012 and projected by CMIP5 model ensemble for a business-as-usual scenario with the Representative Concentration Pathway (RCP) 8.5 until end of the 21st century relative to the reference period of 1971–2000. Error bars denote the 25th and 75th percentiles for the multi-model mean CMIP5 projections for each period spatially across CONUS. Gray shadings mark the projected range of 2021–2099 for spring temperature (dark grey) and summer precipitation anomalies (light grey). Data were extracted for 2012 from NOAA-NCEI (<http://www.ncdc.noaa.gov/cag/time-series/us/>) and for CMIP5 projections from the 2015 ‘NOAA Technical Report NESDIS 144’ (33) (<https://www.cicsnc.org/about/tsu/tr144-data>). The following models were used to calculate the multi-model CMIP5 means in this report: BCC-CSM1.1, CCSM4, CSIRO-Mk3-6-0, FIO-ESM, GFDL-CM3, GFDL-ESM2G, GFDL-ESM2M, GISS-E2-R, HadGEM2-A0, HadGEM2-ES, IPSL-CM5B-LR, IPSL-CM5A-LR, MIROC5, MIROC-ESM-CHEM, MIROC-ESM, and MRI-CGCM3. Please note that these are multi-model mean projections across CONUS, which do not imply consistency among models. Significant trends are based on model agreement (>90%) and at least two standard deviations from the reference period. While significant spring warming is consistently projected across CONUS for all periods, significant trends on summer drying are limited to certain regions: summer drying is projected for most of CONUS (except the East Coast) by mid of the century (2041–2070) and significant drying trends are limited to parts of the Central US (see NESDIS 144, Fig. 32a). By the end of the century (2070–2099), drying is expected to intensify and significant drying trends are projected for large parts of the Northern (Central & West) US, covering in total one-third of CONUS.

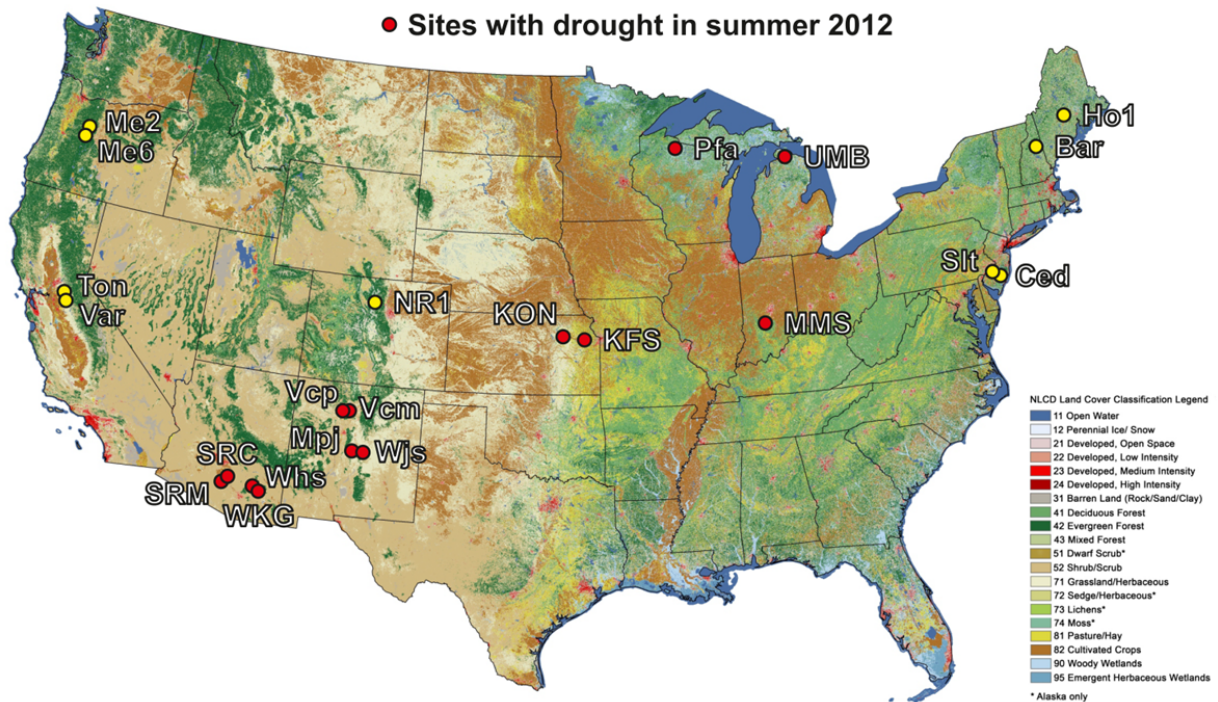


**Fig. S2. Flux tower sites used in this synthesis.** Red points denote sites that experienced drought in summer 2012 (i.e. seasonal precipitation deficit of at least 10% compared to the baseline of 2008–2010). Source base map: National Land Cover Database 2011 (NLCD 2011, <http://www.mrlc.gov/nlcd2011.php>) – see Jin *et al.* 2013 (34) for details. The full names for each site ID can be found in **Table S1**.

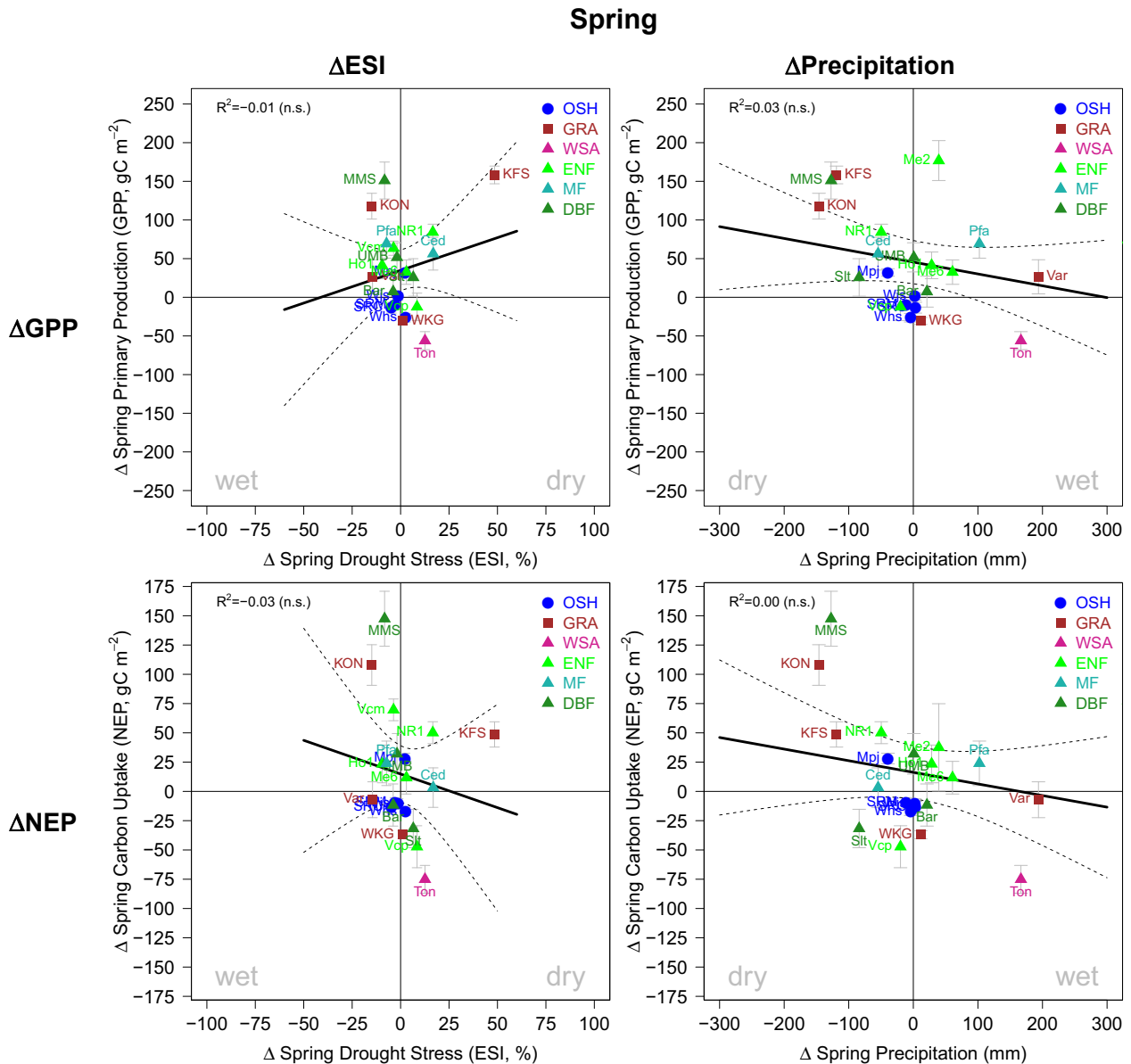


**Fig. S3. Flux tower derived spring anomalies in ecosystem carbon fluxes.** Seasonal anomalies of GPP and NEP during spring related to anomalies in drought stress (via ESI, Evaporative Stress Index) and precipitation in 2012 relative to the baseline of 2008–2010. All regression slopes are not significant (n.s.) and are given for comparison to the main controlling variables during spring (temperature) and summer (ESI). Symbols and colors denote IGBP land-use classes and error bars the uncertainties in the flux anomalies. Dashed lines denote the confidence interval of the ordinary least squares mean regression (bold line).

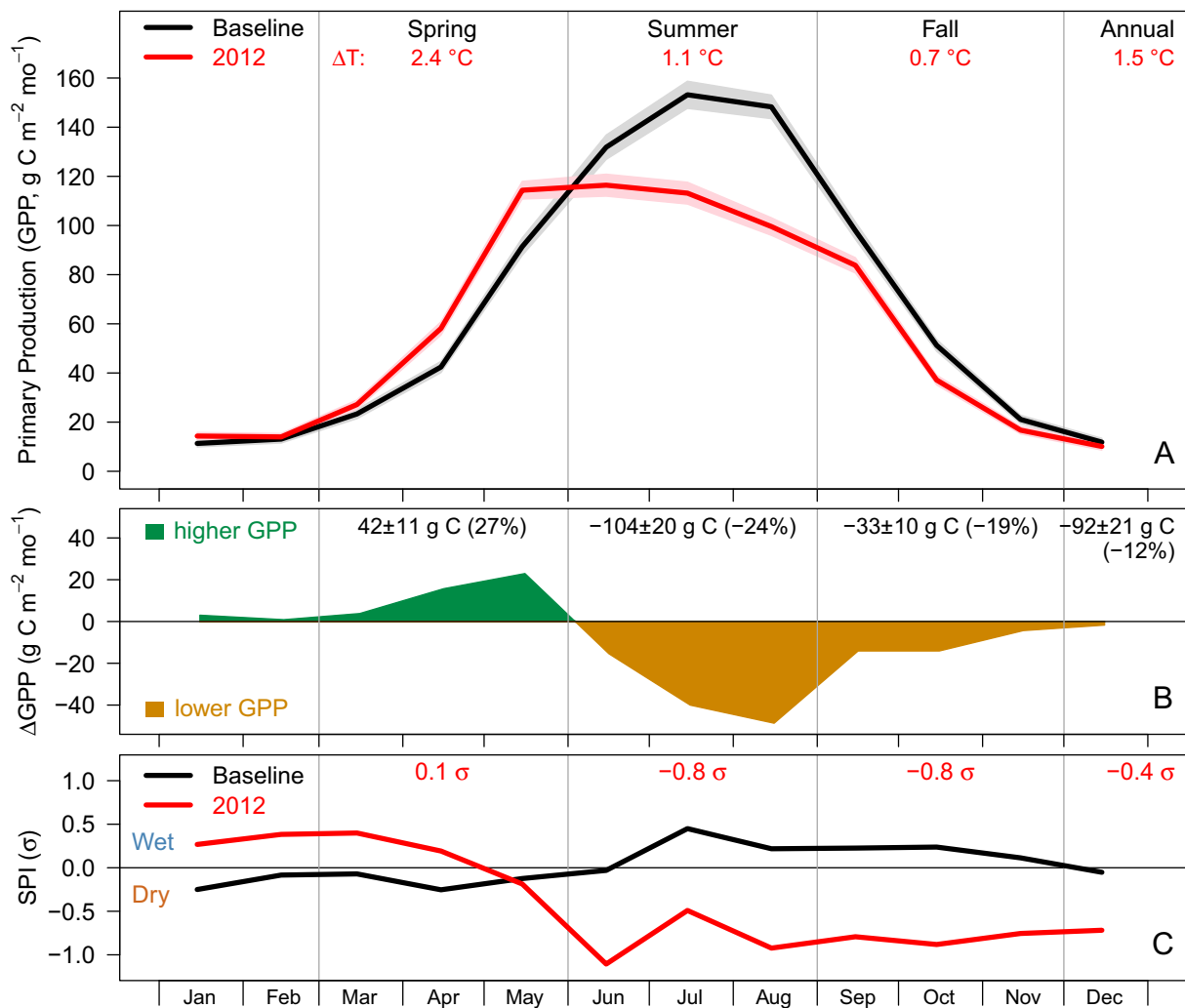


**Fig. S4. The impact of concurrent warming and drought on primary production.** (A) Ensemble mean of eddy-covariance derived monthly gross primary production (GPP) for 2012 (red) and the baseline of 2008–2010 (black) at sites that experienced drought during summer 2012 ( $n=13$ ), and their monthly anomalies (B). Numbers atop denote the mean seasonal anomalies and their uncertainties from Monte-Carlo simulations of monthly fluxes (see also shadings in A). (C) Standardized Precipitation Index (SPI, 6 months,  $\sigma$ ) for 2012 and baseline. Numbers atop denote seasonal means for 2012. Site-scale SPI data was provided by the High Plains Regional Climate Center.



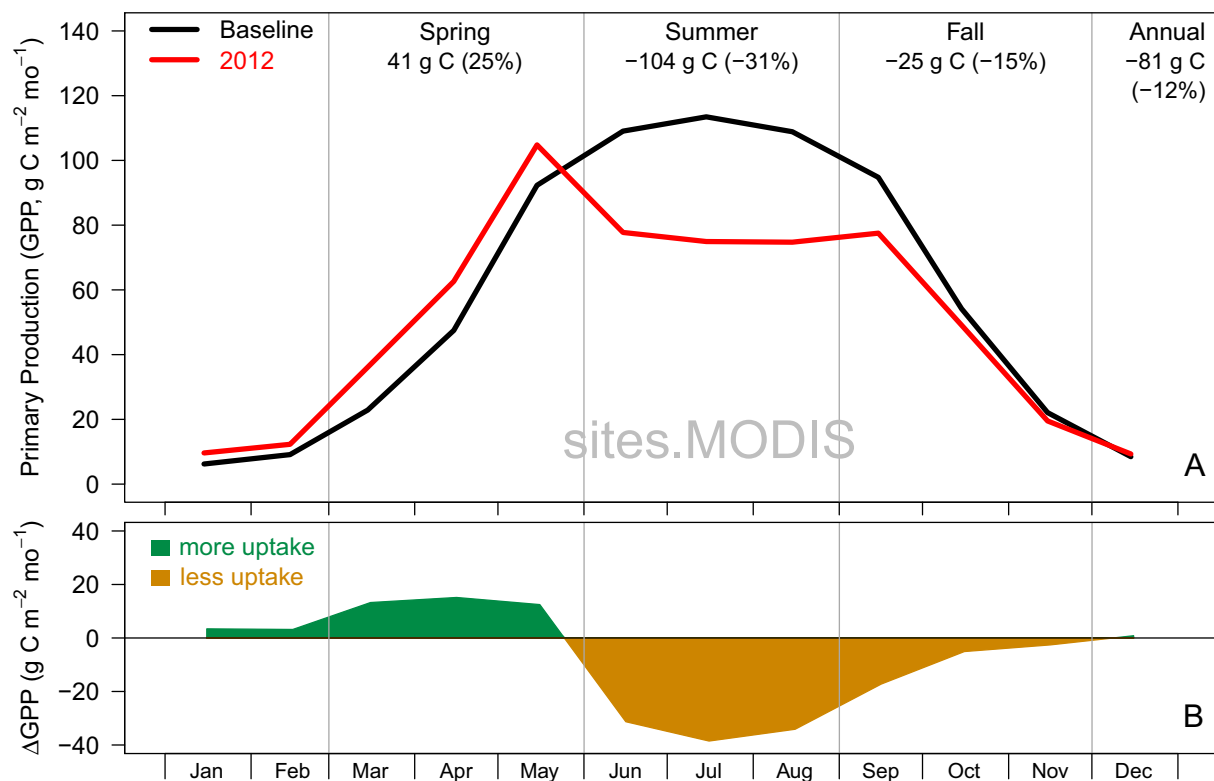


**Fig. S5. The impact of concurrent warming and drought on primary production from MODIS.** (A) Ensemble mean of monthly GPP for 2012 (red) and the baseline of 2008–2010 (black) at flux tower sites that experienced drought during summer 2012 ( $n=13$ ) based on MODIS. Numbers atop denote the mean seasonal anomalies relative to baseline ( $\text{g C m}^{-2}$  and %). (B) Anomalies of 2012 (shading) relative to the baseline.

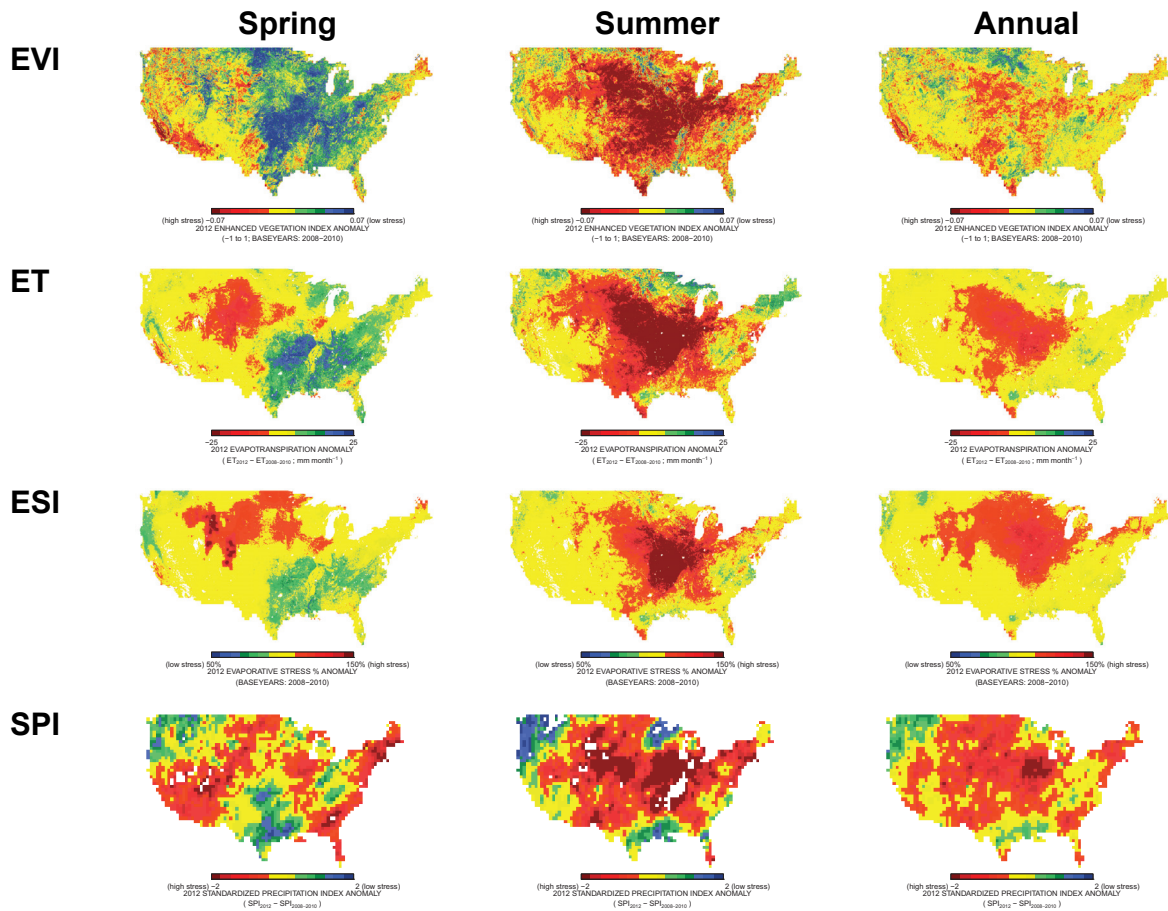


**Fig. S6. Spatial patterns of vegetation activity, evapotranspiration and drought intensity in the US.** Spatial anomalies for enhanced vegetation index (EVI), evapotranspiration (ET), evaporative stress index (ESI) and standardized precipitation index (SPI) during spring (MAM), summer (JJA), and annual in 2012 relative to baseline (2008–2010). Red colors indicate negative anomalies (reductions), while green & blue colors show positive anomalies (increases). Large-scale SPI data were provided by the Global Integrated Drought Monitoring and Prediction System (GIDMaPS) (35).

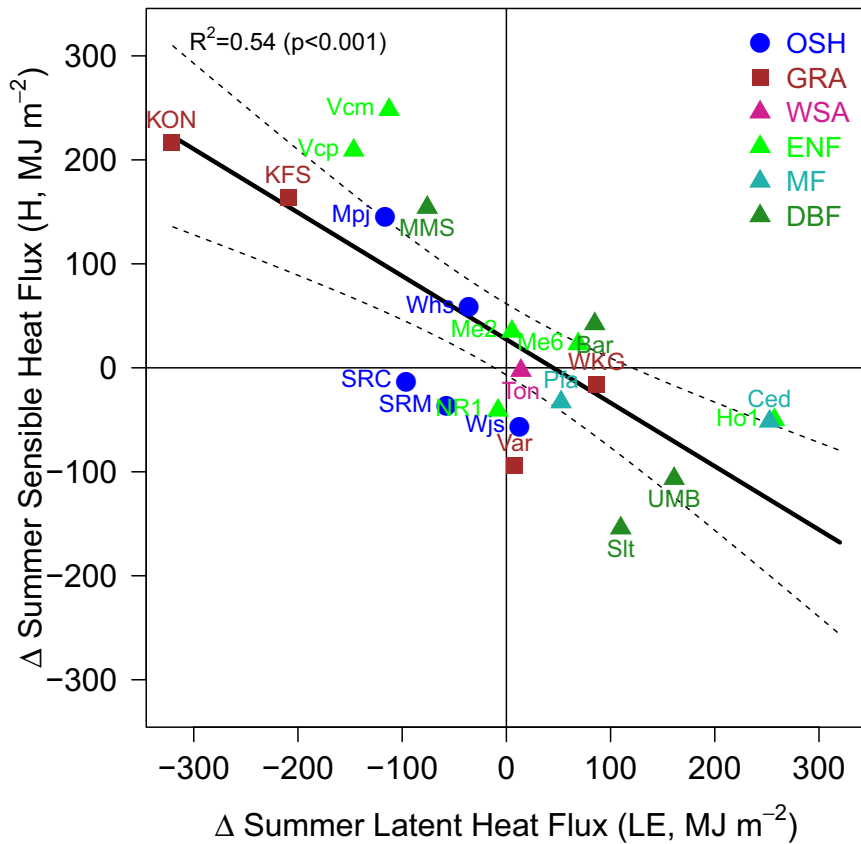


**Fig. S7. The coupling of energy and water fluxes across EC sites during summer.** The relationship of sensible heat flux (H) and latent heat flux (LE) during summer across all sites (n=22) in 2012 relative to the baseline of 2008–2010. Assuming constant available energy, decreases in LE (evaporative cooling) contribute to increases in H and lead to a lower evaporative fraction (relative heating). Symbols and colors denote IGBP land-use classes (see **Table S1**).

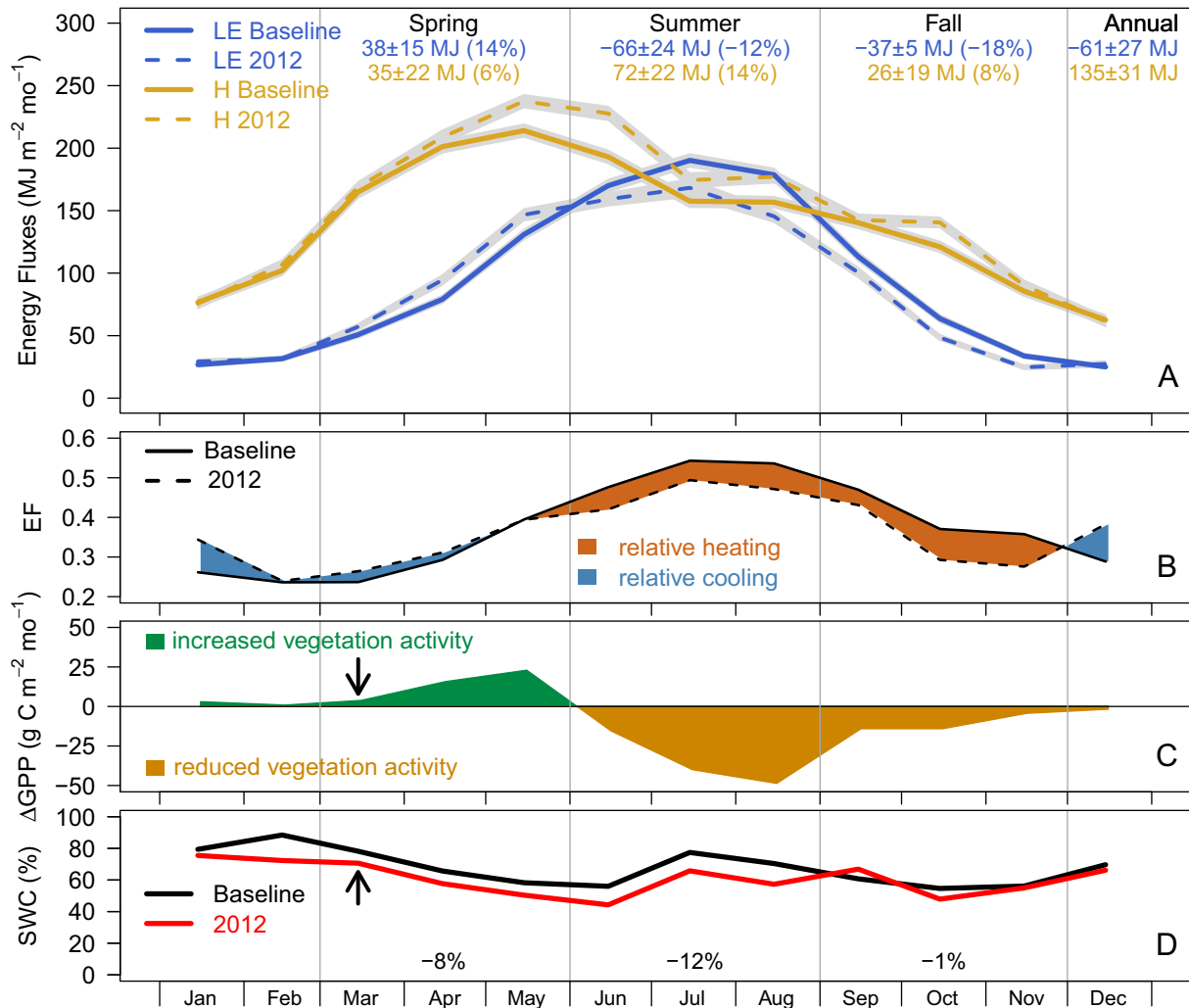


**Fig. S8. The impact of earlier vegetation activity on water and energy fluxes during summer drought.** (A) Ensemble mean of monthly latent heat flux (LE) and sensible heat flux (H) for 2012 and the baseline 2008–2010 from flux tower measurements at sites that experienced drought during summer 2012 ( $n=13$ , see **Table S4**). Numbers atop denote the mean seasonal anomalies and their uncertainties from Monte-Carlo simulations (see also grey shadings). (B) Evaporative fraction (EF) for 2012 and baseline with shadings indicating integrated anomalies. (C) Anomalies of gross primary production (GPP) show earlier vegetation activity inferred by photosynthetic activity in 2012 relative to baseline. Arrows indicate the earlier start of vegetation activity (GPP) and an earlier drawdown in (D) volumetric soil water content (SWC, % of saturation), numbers denote mean seasonal anomalies. SWC data were available for 8 out of the 13 sites only.

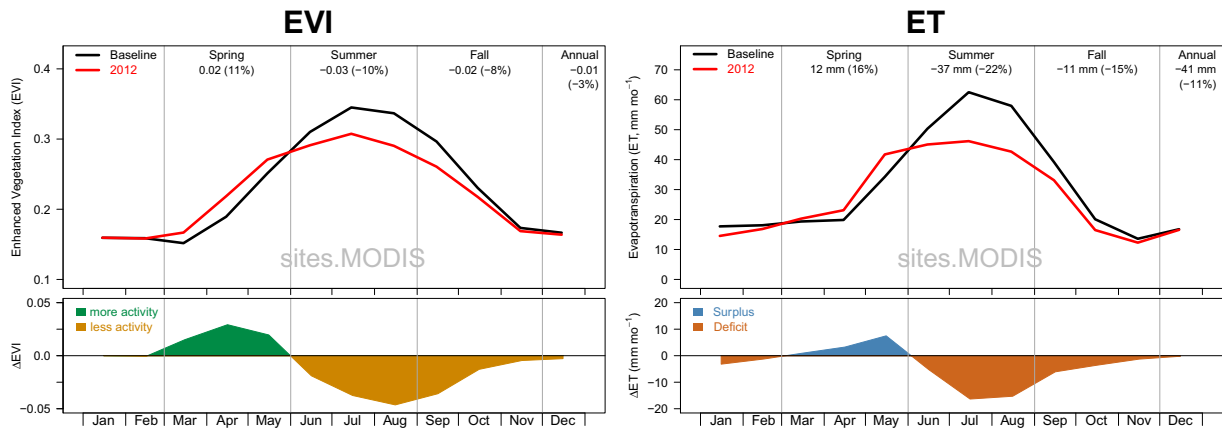


**Fig. S9. The vegetation activity and evapotranspiration from MODIS.** Ensemble mean of monthly enhanced vegetation index (EVI) and evapotranspiration (ET) from MODIS at flux tower sites that experienced drought during summer 2012 ( $n=13$ ). Numbers atop denote the mean seasonal anomalies relative to the baseline. Bottom panels denote the 2012 anomalies (shading) relative to the mean baseline of 2008–2010.

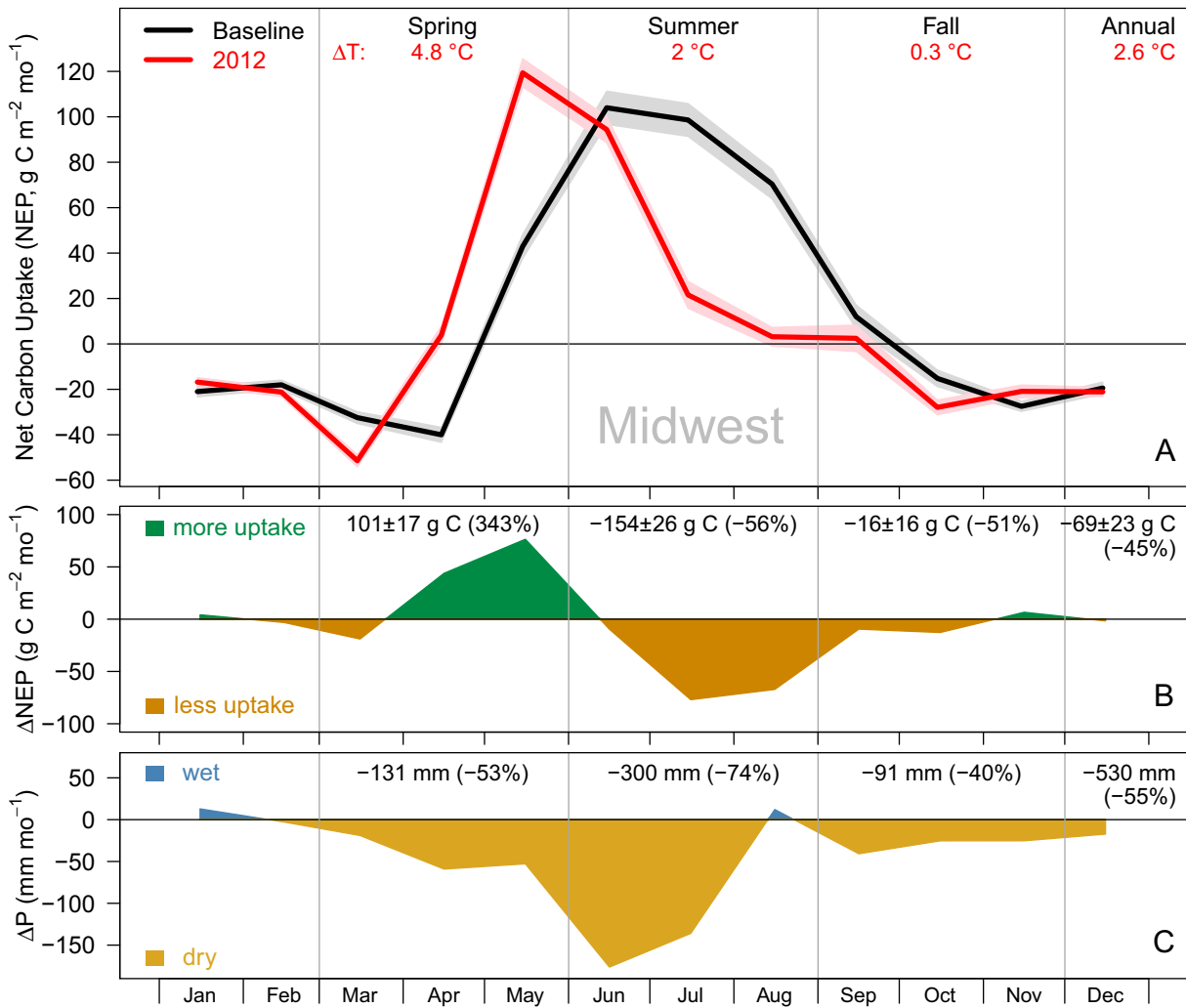


**Fig. S10. Forward shifted net carbon uptake in the Midwest.** (A) Ensemble mean of eddy-covariance derived monthly net ecosystem production (NEP) for 2012 and the baseline of 2008–2010, and the 2012 anomalies (B) in the Midwest ( $n=3$ ). Numbers atop denote the mean seasonal anomalies and their uncertainties from Monte-Carlo simulations (see also shadings in A). (C) Anomalies of monthly precipitation, numbers show absolute (mm) and relative (%) anomalies.

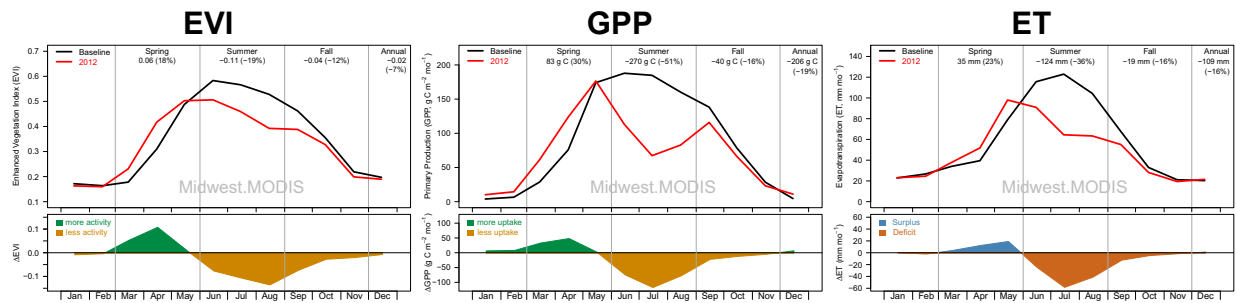


**Fig. S11. The vegetation activity and ecosystem fluxes in the Midwest from MODIS.** Regional ensemble mean of monthly enhanced vegetation index (EVI), gross primary production (GPP) and evapotranspiration (ET) for 2012 and the baseline of 2008–2010 (bold lines) at flux tower locations in the Midwest based on MODIS. The Midwest sites with drought during summer 2012 were KON, KFS, MMS (n=3).

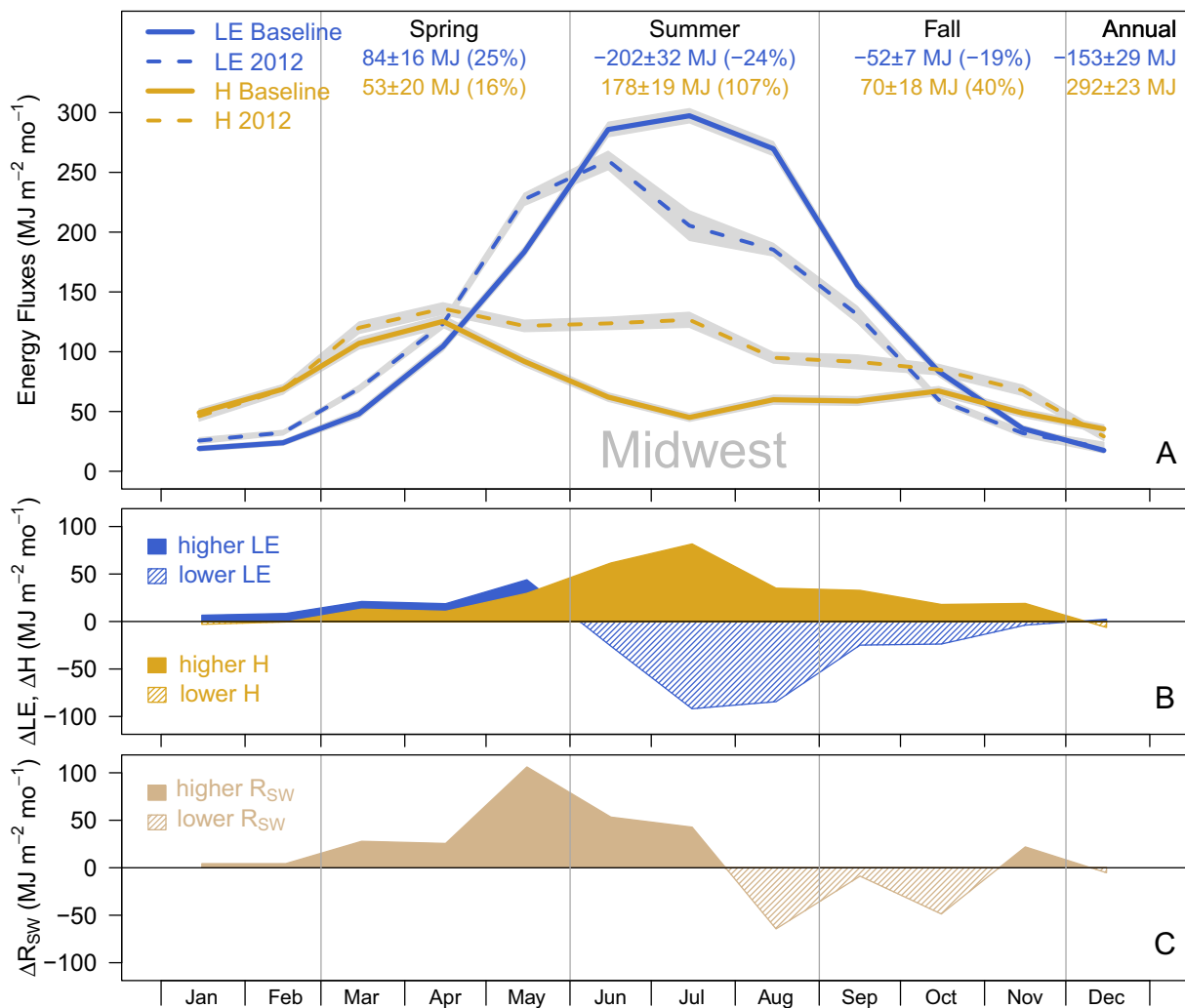


**Fig. S12. The shift in energy fluxes in the Midwest.** (A) Ensemble mean of monthly latent heat flux (LE) and sensible heat flux (H) for 2012 and baseline from flux tower measurements in the Midwest ( $n=3$ , sites US-KON, US-KFS, US-MMS). Numbers atop denote the mean seasonal anomalies and their uncertainties (see also grey shadings) from Monte-Carlo simulations. (B) Anomalies of 2012 are denoted as colored shadings. (C) The anomalies in shortwave incoming radiation ( $\text{R}_{\text{sw}}$ ) in 2012 relative to the baseline of 2008–2010.



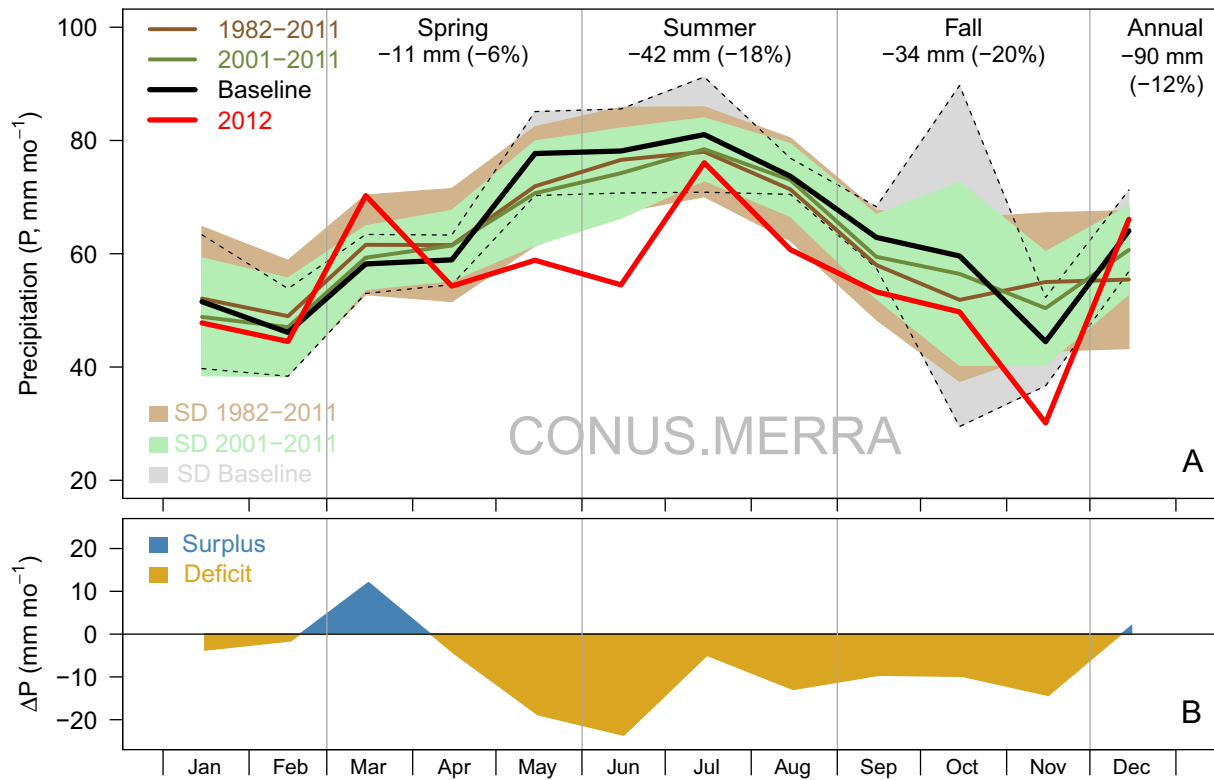


**Fig. S13. Seasonal precipitation variability across the Contiguous US.** (A) MERRA based monthly mean (lines) and standard deviations (SD, shadings) of precipitation across CONUS for the periods 1982–2011, 2001–2011, the baseline of 2008–2010 and in 2012. Dashed black lines denote the SD-range of the baseline and numbers atop show mean seasonal anomalies. (B) The anomalies in 2012 relative to the baseline of 2008–2010.

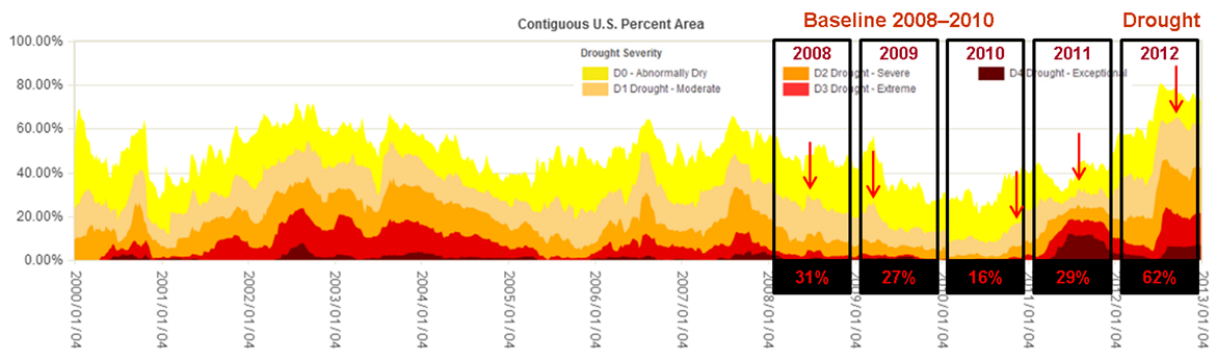


**Fig. S14. The percentage area of drought across the Contiguous US.** Modified from NCDC/NOAA ([www.ncdc.noaa.gov/sotc/drought/2012/13](http://www.ncdc.noaa.gov/sotc/drought/2012/13)). Boxes mark the years 2008 to 2012 with the maximum percentage of total area affected by moderate to extreme drought (see arrows for seasonal timing), based on the Palmer Drought Severity Index (PDSI). The absolute maximum of 80% was reached during the ‘Dust Bowl’ period in July 1934. Based on dry *versus* wet areas from PDSI (see [www.ncdc.noaa.gov/extremes/cei/graph/3/01-12](http://www.ncdc.noaa.gov/extremes/cei/graph/3/01-12)), the year 2012 was the 4<sup>th</sup> most extreme dry year since 1910 (after 1934, 1954, 1956) and the driest year since 1956. The subsequent baseline years of 2008 to 2010 were relatively close to the long-term mean across CONUS. The year 2011 was extremely dry in the South and Southwest and was excluded from the baseline to avoid confounding effects.

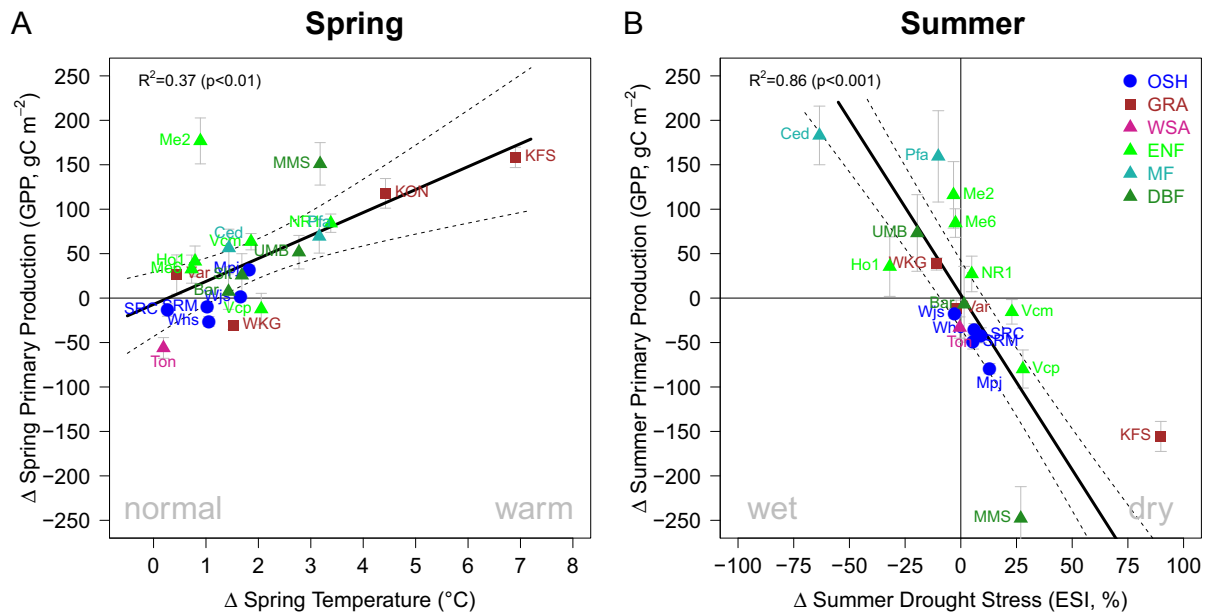


**Fig. S15. The effect of seasonal climate anomalies on primary production in 2012.** Flux tower derived seasonal anomalies of gross primary production (GPP) during spring (A, related to temperature) and summer (B, related to drought stress via ESI, Evaporative Stress Index) in 2012 relative to the baseline of 2008–2010. Symbols and colors denote IGBP land-use classes (see **Table S1**) and error bars the uncertainties in the flux anomalies. Dashed lines denote the confidence interval of the ordinary least squares mean regression (bold line). The summer anomaly at the site KON is out of scale (see **Table S10**) and was omitted from display in this figure, but was included in the regression analysis.

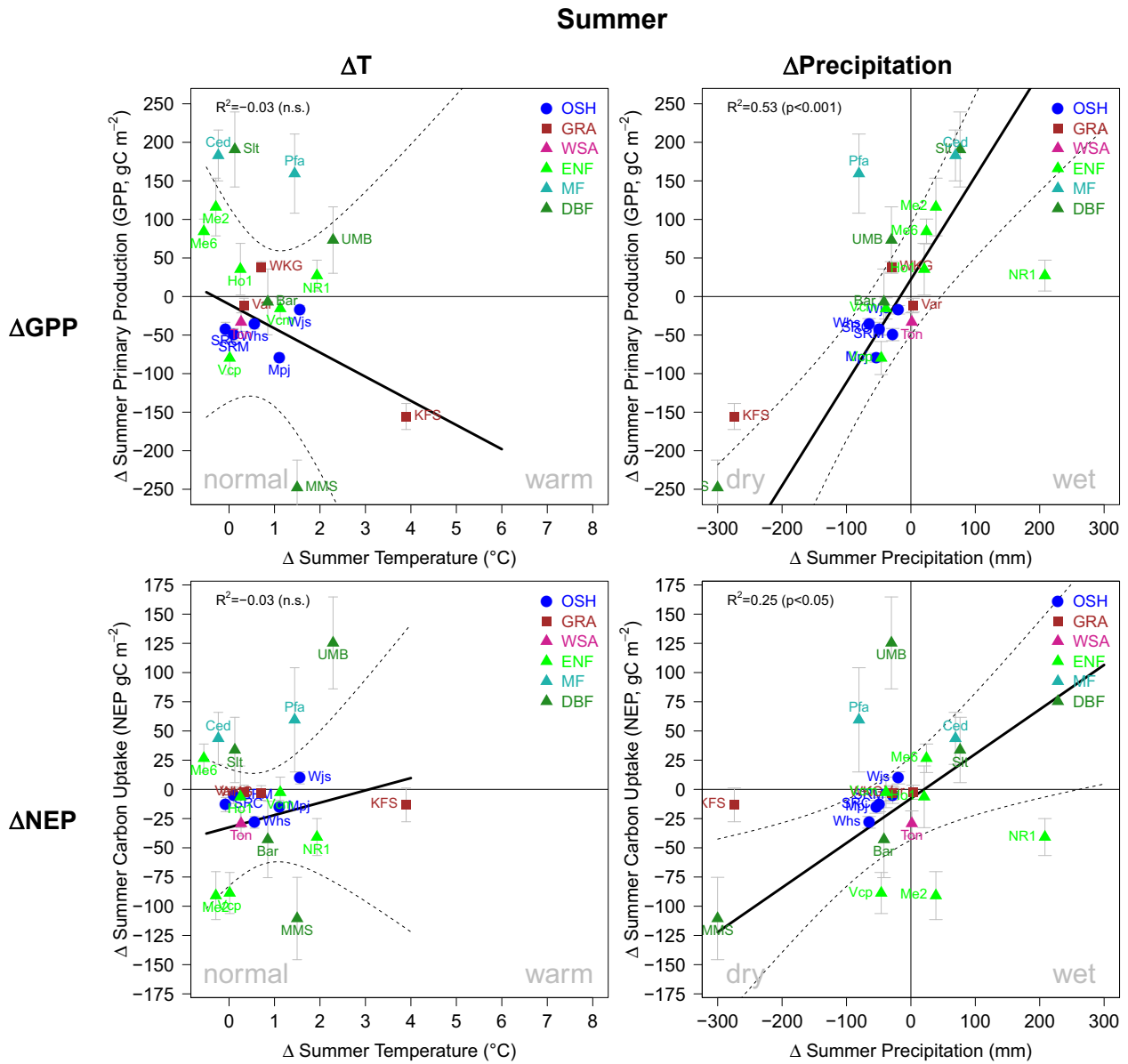


**Fig. S16. Flux tower derived summer anomalies in ecosystem carbon fluxes.** Seasonal anomalies of GPP and NEP during summer related to anomalies in temperature and precipitation in 2012 relative to the baseline of 2008–2010. The regression slopes for temperature are not significant (n.s.). Both variables are given for comparison to the main controlling variables during spring (temperature) and summer (ESI). Symbols and colors denote IGBP land-use classes and error bars the uncertainties in the flux anomalies. Dashed lines denote the confidence interval of the ordinary least squares mean regression (bold line). The summer GPP and NEP anomalies at the site KON are out of scale (see **Table S10**) and were omitted from display in this figure, but were included in the regression analyses.

## Supporting References

1. Baldocchi D (2014) Measuring fluxes of trace gases and energy between ecosystems and the atmosphere – the state and future of the eddy covariance method. *Glob. Change Biol.* 20(12):3600-3609.
2. Hargrove WW, Hoffman FM, & Law BE (2003) New analysis reveals representativeness of the AmeriFlux network. *EOS, Transactions American Geophysical Union* 84(48):529-535.
3. Omernik JM (1987) Ecoregions of the conterminous United States. *Ann. Assoc. Am. Geogr.* 77(1):118-125.
4. Leuning R, van Gorsel E, Massman WJ, & Isaac PR (2012) Reflections on the surface energy imbalance problem. *Agric. For. Meteorol.* 156(0):65-74.
5. CarbonTracker (2015) CarbonTracker CT2013B. <http://carbontracker.noaa.gov>.
6. Peters W, *et al.* (2007) An atmospheric perspective on North American carbon dioxide exchange: CarbonTracker. *Proc. Natl. Acad. Sci. U. S. A.* 104(48):18925-18930.
7. Peters W, *et al.* (2010) Seven years of recent European net terrestrial carbon dioxide exchange constrained by atmospheric observations. *Glob. Change Biol.* 16(4):1317-1337.
8. Hoerling M, *et al.* (2014) Causes and Predictability of the 2012 Great Plains Drought. *Bulletin of the American Meteorological Society* 95(2):269-282.
9. Hoerling M, Schubert S, & Kingtse M (2013) An Interpretation of the Origins of the 2012 Central Great Plains Drought. (NOAA Drought Task Force), p 47.
10. Blunden J & Arndt DS (2013) State of the Climate in 2012. *Bulletin of the American Meteorological Society* 94(8):S1-S258.
11. NOAA (2015) Billion-Dollar U.S. Weather and Climate Disasters (National Oceanic and Atmospheric Administration (NOAA), National Centers for Environmental Information (NCEI), <http://www.ncdc.noaa.gov/billions/events>).
12. Baldocchi D & Ma S (2013) How will land use affect air temperature in the surface boundary layer? Lessons learned from a comparative study on the energy balance of an oak savanna and annual grassland in California, USA. *Tellus B* 65:19994.
13. Miralles DG, Teuling AJ, van Heerwaarden CC, & Vila-Guerau de Arellano J (2014) Mega-heatwave temperatures due to combined soil desiccation and atmospheric heat accumulation. *Nature Geosci* 7(5):345-349.
14. Yamori W, Hikosaka K, & Way DA (2014) Temperature response of photosynthesis in C3, C4, and CAM plants: temperature acclimation and temperature adaptation. *Photosynth Res* 119(1):101-117.
15. van der Molen MK, *et al.* (2011) Drought and ecosystem carbon cycling. *Agric. For. Meteorol.* 151(7):765-773.
16. Scott RL, Hamerlynck EP, Jenerette GD, Moran MS, & Barron-Gafford GA (2010) Carbon dioxide exchange in a semidesert grassland through drought-induced vegetation change. *Journal of Geophysical Research: Biogeosciences* 115(G3):G03026.
17. Thomas CK, *et al.* (2009) Seasonal hydrology explains interannual and seasonal variation in carbon and water exchange in a semiarid mature ponderosa pine forest in central Oregon. *Journal of Geophysical Research: Biogeosciences* 114:G04006.
18. Brzostek ER, *et al.* (2014) Chronic water stress reduces tree growth and the carbon sink of deciduous hardwood forests. *Glob. Change Biol.* 20(8):2531-2539.

19. Clark KL, Skowronski NS, Gallagher MR, Renninger H, & Schäfer KVR (2014) Contrasting effects of invasive insects and fire on ecosystem water use efficiency. *Biogeosciences* 11(23):6509-6523.
20. Hollinger DY, *et al.* (2004) Spatial and temporal variability in forest-atmosphere CO<sub>2</sub> exchange. *Glob. Change Biol.* 10(10):1689-1706.
21. Jenkins JP, *et al.* (2007) Refining light-use efficiency calculations for a deciduous forest canopy using simultaneous tower-based carbon flux and radiometric measurements. *Agric. For. Meteorol.* 143(1–2):64-79.
22. Gough CM, *et al.* (2013) Sustained carbon uptake and storage following moderate disturbance in a Great Lakes forest. *Ecol. Appl.* 23(5):1202-1215.
23. Desai A (2014) Influence and predictive capacity of climate anomalies on daily to decadal extremes in canopy photosynthesis. *Photosynth Res* 119(1-2):31-47.
24. Brunsell NA, Nippert JB, & Buck TL (2014) Impacts of seasonality and surface heterogeneity on water-use efficiency in mesic grasslands. *Ecohydrology* 7(4):1223-1233.
25. Anderson-Teixeira KJ, Delong JP, Fox AM, Brese DA, & Litvak ME (2011) Differential responses of production and respiration to temperature and moisture drive the carbon balance across a climatic gradient in New Mexico. *Glob. Change Biol.* 17(1):410-424.
26. Sanchez-Mejia ZM & Papuga SA (2014) Observations of a two-layer soil moisture influence on surface energy dynamics and planetary boundary layer characteristics in a semiarid shrubland. *Water Resour. Res.* 50(1):306-317.
27. Scott RL, Jenerette GD, Potts DL, & Huxman TE (2009) Effects of seasonal drought on net carbon dioxide exchange from a woody-plant-encroached semiarid grassland. *Journal of Geophysical Research: Biogeosciences* 114(G4):G04004.
28. Scott RL (2010) Using watershed water balance to evaluate the accuracy of eddy covariance evaporation measurements for three semiarid ecosystems. *Agric. For. Meteorol.* 150(2):219-225.
29. Ma S, Baldocchi DD, Xu L, & Hehn T (2007) Inter-annual variability in carbon dioxide exchange of an oak/grass savanna and open grassland in California. *Agric. For. Meteorol.* 147(3–4):157-171.
30. Monson RK, *et al.* (2002) Carbon sequestration in a high-elevation, subalpine forest. *Glob. Change Biol.* 8(5):459-478.
31. Vickers D, Thomas CK, Pettijohn C, Martin JG, & Law BE (2012) Five years of carbon fluxes and inherent water-use efficiency at two semi-arid pine forests with different disturbance histories. *Tellus Ser. B-Chem. Phys. Meteorol.* 64:14.
32. Ruehr NK, Law BE, Quandt D, & Williams M (2014) Effects of heat and drought on carbon and water dynamics in a regenerating semi-arid pine forest: a combined experimental and modeling approach. *Biogeosciences* 11(15):4139-4156.
33. Sun L, *et al.* (2015) Regional Surface Climate Conditions in CMIP3 and CMIP5 for the United States: Differences, Similarities, and Implications for the U.S. National Climate Assessment, NOAA Technical Report NESDIS 144. p 111.
34. Jin S, *et al.* (2013) A comprehensive change detection method for updating the National Land Cover Database to circa 2011. *Remote Sensing of Environment* 132:159-175.
35. Hao Z, AghaKouchak A, Nakhjiri N, & Farahmand A (2014) Global integrated drought monitoring and prediction system. *Scientific Data* 1.